UNIVERSITÀ DEGLI STUDI DI CATANIA

DOTTORATO DI RICERCA IN FISICA

ROSARIO GIANLUCA PIZZONE

ELECTRON SCREENING EFFECTS ON FUSION REACTIONS

TESI PER IL CONSEGUIMENTO DEL TITOLO

XIV CICLO 1998-2001

UNIVERSITÀ DEGLI STUDI DI CATANIA

DOTTORATO DI RICERCA IN FISICA

ROSARIO GIANLUCA PIZZONE

ELECTRON SCREENING EFFECTS ON FUSION REACTIONS

Coordinatore del corso: Prof. F. Catara

Supervisore: Prof. C. Spitaleri

TESI PER IL CONSEGUIMENTO DEL TITOLO

XIV CICLO 1998-2001

Verso le stelle, lontane e nascoste,

il mio sguardo ho rivolto, la notte,

ma nello specchio le risposte ho trovato,

a domande da sempre taciute:

cercavo il mondo, ho trovato me stesso.

Contents

Introduction

Several astrophysical contexts, from the Big Bang nucleosynthesis to the energy production in stars, cannot be studied without precise measurements (precisions $\sim$5%) of few crucial reaction cross sections [Rolfs & Rodney (1988)].

These must be carried on at energies relevant for astrophysics, the Gamow window, which are generally very low (1-100 keV) in comparison to the Coulomb barrier ($\geq$1 MeV) for charged-particle-induced reactions. The presence of such a barrier causes an exponential decrease for the cross section with decreasing energy which leads to a low signal-to-noise ratio and consequently to a low-energy limit of direct cross section measurements, usually larger than the Gamow energy of astrophysical interest. In these cases what is usually done is to extrapolate the available experimental data to zero energy by means of theoretical arguments (e.g. R-Matrix fit).

Recently, the development of new experimental facilities, such as LUNA at Laboratori Nazionali del Gran Sasso, together with improved targets and detection techniques, allowed for cross section measurements at energies as low as the Gamow window ones (e.g. [Bonetti et al. (1999)]).

In spite of these efforts measurements at ultra-low energies suffer from the complication due to the effects of electron screening [Assenbaum et al. (1987)]. As it will be stressed in chapter two the electron screening effect represents one of the most important problems in nuclear astrophysics. The necessity, for astrophysical reaction networks, to know the bare nucleus cross section (mainly because the stellar screening is different from the one in laboratory) requires the electron screening effect in the laboratory to be fully understood; this result is still far to be achieved and a number of recent experimental results are not explained using the available theoretical models. A better understanding of electron screening can also help in developing more reliable atomic models. It is important to underline that direct measurements of the electron screening potential are generally performed via an extrapolation, whose reliability decreases with increasing unexplored energetic region [Fiorentini et al. (1995)].

Thus many alternative methods have been proposed in order to retrieve informations on the bare nucleus cross sections (for instance the Coulomb dissociation [Baur & Rebel (1994)] and transfer reactions [Gagliardi et al. (1999)]). Among these methods the Trojan Horse Method (THM) [Baur (1986)] seems to be particularly suited for extracting information on charged-particle-induced reaction cross sections. As it will be pointed out extensively in chapter three, the method allows to extract the bare nucleus cross section without any extrapolation. It represents a complementary method for experimental nuclear astrophysics because normalization to direct data above the Coulomb barrier is always needed.

The THM is based on a quasi-free break-up process and allows to extract the cross section of a two-body reaction (of astrophysical interest)

$$a + x \rightarrow c + C$$

from a suitable three body one

$$a + A \rightarrow c + C + s\,.$$

In this notation the particle A, the "Trojan Horse", which can be either the projectile or the target nucleus, has a high probability to be clustered into x and s, i.e. $A = x \oplus s$. Particle x acts as a participant to the two body reaction, while s keeps the role of spectator. If the energy in the entrance channel is higher than the Coulomb barrier, then the interaction between x and a proceeds directly in the nuclear interaction zone, thus by-passing the Coulomb barrier.

An improved theoretical formalism, based on a Distorted Wave Born Approximation (DWBA) [Typel & Wolter (2000)], will also be introduced in chapter 3. This will allow the extraction of the energy trend for the bare nucleus astrophysical factor whose absolute normalization must be performed via a comparison with direct data at energies above the Coulomb barrier, where the THM and the direct results must be equivalent.

The method has been applied to measure the bare nucleus astrophysical S(E)-factor of two important lithium depleting reactions, the $^{6}Li(d,\alpha)^{4}He$ and the $^{7}Li(p,\alpha)^{4}He$, and hence the electron screening potential for both reactions.

This work will be organized as follows.

The primordial nucleosynthesis and the lithium problem, are presented in chapter one. During primordial nucleosynthesis only elements with A$\leq$7 were formed [Malaney & Mathews (1993)]. Among these isotopes, lithium has been studied both observationally and theoretically in the last decades [Michaud & Charbonneau (1991)]. The determination of the primordial lithium abundance allows, via the comparison with theoretical calculations, to get estimates on the important cosmological parameter η, which is strictly connected with the baryon density of the Universe [Vangioni-Flam et al. (2000)]. This procedure requires, among other fulfillments, a detailed knowledge of lithium producing and depleting mechanisms.

In particular the key role of the reaction $^{7}Li(p,\alpha)^{4}He$ will be acknowledged in this thesis, together with other reactions involving lithium isotopes. The indetermination on this cross section is one of the main sources of uncertainty in this field.

In chapter two the main difficulties for the experimental measurements in nuclear astrophysics will be briefly introduced together with the most useful concepts and definitions. A particular attention will be devoted to the role of atomic electron clouds, whose influence at these energies must be taken into account in retrieving informations from experiments [Assenbaum et al. (1987)]. This is because of the electron screening effect which essentially enhances the cross section with decreasing incident energy.

In order to by-pass the difficulties arising from measuring the bare nucleus cross section via direct experiments many indirect methods have been proposed and the

Trojan Horse Method (THM) [Baur (1986)] among them. Chapter three will be focused on a theoretical introduction and its previous applications. The principles of the method will also been given together with the limits of its applicability. The THM allows to extract the bare astrophysical factor without extrapolation, but, because of the normalization procedure, it represents a complementary tool to direct measurements.

The THM has been applied to the $^6Li(d,\alpha)^4He$ reaction [Cherubini et al. (1996), Spitaleri et al. (2001)] and the $^7Li(p,\alpha)^4He$ [Calvi et al. (1997), Spitaleri et al. (1999), Lattuada et al. (2001)] reaction, which are important for lithium depletion problem in different astrophysical scenarios. The information was extracted from the $^6Li(^6Li,\alpha\alpha)^4He$ and the $^7Li(d,\alpha\alpha)n$ three body reactions, respectively. Chapter four and five will be devoted to their complete experimental study. For both reactions the bare nucleus S(E)-factor and the electron screening potential have been measured and the results extracted via the THM are compared and normalized to the direct ones taken from [Engstler et al. (1992)].

The electron screening potential obtained in such a way is compared (chapter 6) with the theoretical value predicted in the adiabatic approximation and with other direct determinations. Moreover, in order to verify the assumption that the electron screening depends only on the atomic number of the element and is independent from its mass number, results extracted from $^6Li(d,\alpha)^4He$ and $^7Li(p,\alpha)^4He$ are compared.

The astrophysical implications of the present THM measurement of the $^7Li(p,\alpha)^4He$ reaction are briefly discussed in chapter seven. In particular the attention will be focused on the solar lithium problem, which is, by far, the best studied case of lithium depletion. The THM value of the $^7Li(p,\alpha)^4He$ astrophysical factor will be used as an input value for a stellar evolutionary code (the FRANEC code). The results will be compared with the ones obtained using the NACRE [Angulo et al. (1999)] compilation for both the pre-main-sequence and main sequence phases of Solar evolution.

Chapter 1

The importance of Lithium isotopes in Astrophysics

Lithium plays a special role in Astrophysics since it is produced in primordial nucleosynthesis and destroyed at relatively low temperatures in stars ($T \sim 2 \cdot 10^6$). Because it is formed soon after the Big Bang, its abundance becomes an important cosmological indicator. Because of its stellar destruction, it becomes a useful tracer for particle transport in stars and stellar evolution, as we will review at the end of this chapter. Moreover, in order to use lithium abundances as a cosmological indicator, a complete understanding of its stellar abundances is needed, thus linking the two aspects.

This chapter will be devoted to present the role of lithium in primordial nucleosynthesis as well as the lithium depletion.

1.1 Basic properties of primordial nucleosynthesis

Over the last two decades Big Bang nucleosynthesis (BBN) has emerged as one of the cornerstones of the Big Bang, joining the Hubble expansion and the cosmic microwave background radiation (CBR) in this role. Among them, Big Bang nucleosynthesis probes the Universe to the earliest times, from a fraction of a second to hundreds of seconds. Since BBN involves events that occurred at temperature of order 1 MeV, it naturally plays a key role in forging the connection between cosmology and nuclear physics [Schramm & Turner (1998)].

Standard Big Bang model has the very powerful feature that prediction for the light elements' production is primarily dependent only on one free parameter, the baryon-to-photon ratio η (as we will see in the following pages, it is connected to the baryon density of the Universe). Starting from this, observationally-measured primordial abundances can be fitted up to 10 orders of magnitudes. In picture 1.1 the primordial nucleosynthesis reaction network is reported: the absence of stable nuclei with A=5 or A=8, together with the increasing Coulomb barrier for reactions between heavier nuclei substantially stops the cosmological production in correspondence of ^7Li in Standard Big Bang Nucleosynthesis (SBBN). According to the Standard Big Bang model [Malaney & Mathews (1993)] for $T \leq 10^9$ K it is possible the formation of light nuclei ($^2H,^3He,^4He,^6Li,^7Li$) from the starting chemical species, protons and neutrons. Consistent amounts of these primordially synthesized elements should be found nowadays in appropriate astrophysical contexts.

In this way a comparison between theoretically calculated yields and observed primordial abundances of such elements can be performed in order to test the SBBN. Moreover it is possible [Copi et al. (1995)] to infer hints on the relevant cosmological parameter η from this comparison as shown in figure 1.2. In fact the observed primordial abundances of light nuclides, $^2H,^3He,^4He,^7Li$, can constrain the free

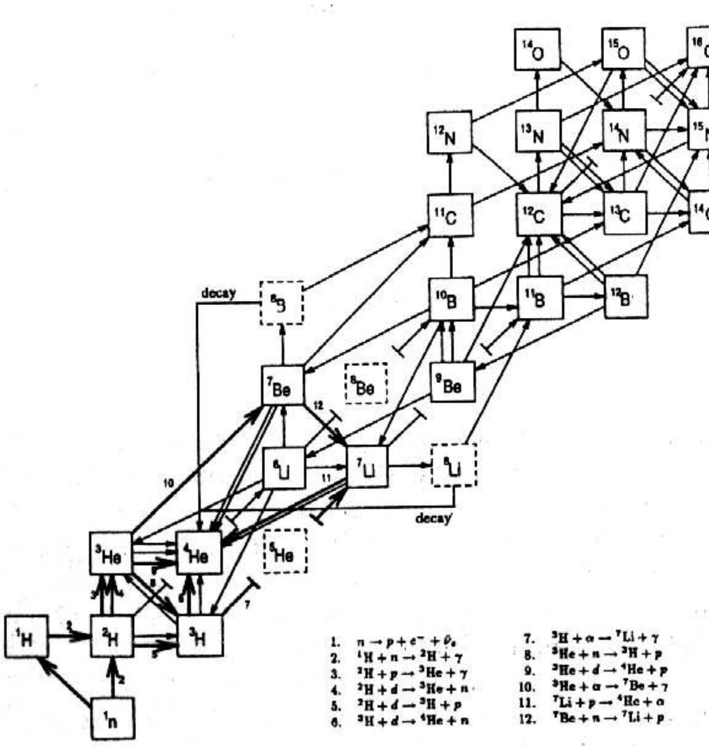

Figure 1.1: The primordial nucleosynthesis reaction network. Dotted squares show the location of A=5,8 instable nuclei.

parameter η so that

$$2.5 \times 10^{-10} \leq \eta \leq 6 \times 10^{-10} \tag{1.1}$$

1.1.1 Primordial abundances of light elements

Let us give some informations about primordial abundances measurements for ^2H, ^3He, ^4He, ^7Li nuclei. We stress that the choice of an appropriate astrophysical environment for the determination of primordial abundances of such nuclides is as difficult as their experimental measurements.

Deuterium - From deuterium abundances in the interstellar medium [Linsky et al. (1993)]

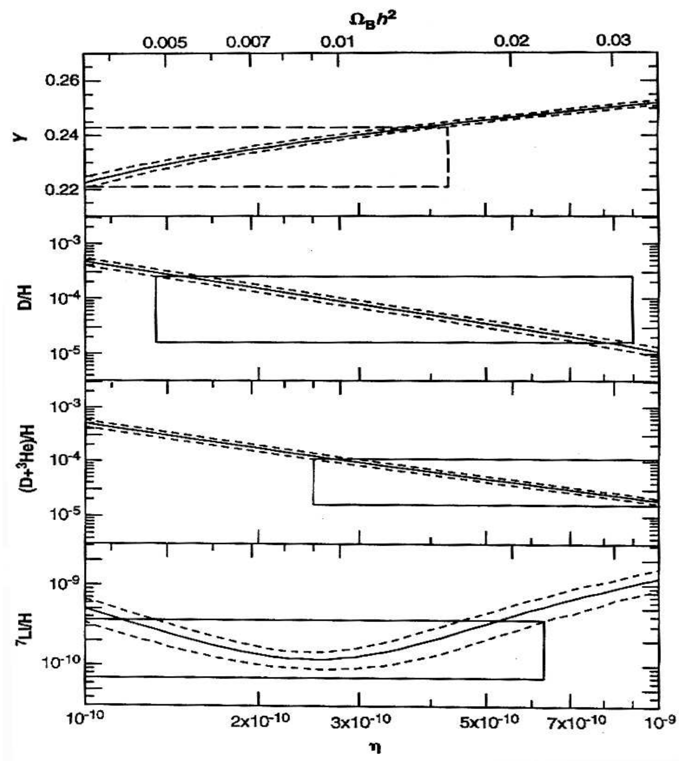

Figure 1.2: Comparison between observed primordial abundances and calculated yields for $^2H,^3He,^4He,^7Li$. Dotted lines show the theoretical uncertainties; in lithium case the uncertainty mainly depends on the cross-section for $^7Li+p \to \alpha+\alpha$ reaction.

a primordial value (expressed in mass fraction[1])

of

$$X_D \geq 1.65^{+0.07}_{-0.18} \times 10^{-5}$$

is extracted.

Deuterium+Helium3 - To take into account that primordial deuterium can be easily burned, in the interstellar medium, via reaction $d+p \to {}^3He+\gamma$, the

[1]The notation X_A, the mass fraction of element A with respect to hydrogen, is often used.

combined abundance of ^2H and ^3He is considered; this value has been measured and yields [Yang et al. (1984)]:

$$X_{D+^3He} \leq 1.1 \times 10^{-4}$$

Helium4 - ^4He-abundance measurements are encouraged thanks to the presence of helium in all the astrophysical environments though the observation of primordial helium is quite a hard task. Moreover stellar production of ^4He can greatly increase its measured abundance. Observations in extremely metal-poor environments, such as extra-galactic HII regions[2], yield a primordial value of [Olive & Steigman (1995)]:

$$Y_p = 0.232 \pm 0.003 \pm 0.005$$

where Y_p is the primordial ^4He mass-fraction[3], the first error is statistical and the second one is systematic.

Lithium - The amount of primordial lithium is still an open question. We refer to [Michaud & Charbonneau (1991)] to have a general overview. By taking as the lithium primordial value the mean of results by [Spite & Spite (1982), Thorburn et al. (1994)] we have

$$X_{^7Li} = (1.4 \pm 0.3^{+1.8}_{-0.4}) \times 10^{-10}$$

where the first error is statistical and the second one is systematic.

Recently a primordial amount of ^6Li has been detected in few halo stars [Lemoine et al. (1997)] and its abundance is about the 5% with respect to ^7Li. For this reason ^6Li can provide an additional constraint on η and, in the meanwhile, can provide a strong lower limit for the ^7Li abundance [Nollet et al. (1997)].

[2]For HII region astrophysicists mean a cloud of fully ionized hydrogen

[3]The notation Y for helium mass abundance is equivalent to X_{He}

1.1.2 From the baryon-to-photon ratio, η, to the baryon density

The determination of a range of variability for the η parameter can provide limits to the baryon density of the Universe. The baryon-to-photon ratio η is defined as

$$\eta = \frac{n_B}{n_\gamma}$$

where n_B and n_γ are the baryon and the photon number density, respectively. If we consider [Copi et al. (1995)] the baryon density, ρ_B we have

$$\rho_B = m_p n_B = m_p \eta n_\gamma$$

where m_p is the proton mass. Considering that all the photons are within the CBR we can write that

$$n_\gamma = \alpha T_0^3$$

with α constant and T_0 the present day CBR temperature ($T_0 = 2.726 \pm 0.005$ K [Mather et al. (1994)]). Hence we find that

$$\rho_B = m_p \eta \alpha T_0^3$$

so that if we introduce the critical density[4] ρ_c

$$\rho_c = \frac{3H^2}{8\pi G}$$

where G is the gravitational constant and H the Hubble parameter, we obtain the adimensional baryon density

$$\Omega_B = \frac{\rho_B}{\rho_c} \tag{1.2}$$

In this way the constraint on η derived from primordial nucleosynthesis become a constraint on Ω_B; for values reported in 1.1 we find that

$$0.01 \leq \Omega_B \leq 0.10$$

[4]This is the limit density for which an isotropic and homogeneous Universe collapses

Estimates of "luminous matter" show [Bahcall et al. (1995)] that most baryonic matter is "dark". Besides from measurements of total matter density Ω_M, it is found [Bahcall et al. (1995)] $\Omega_M \geq 0.3$. These results can be seen in picture 1.3.

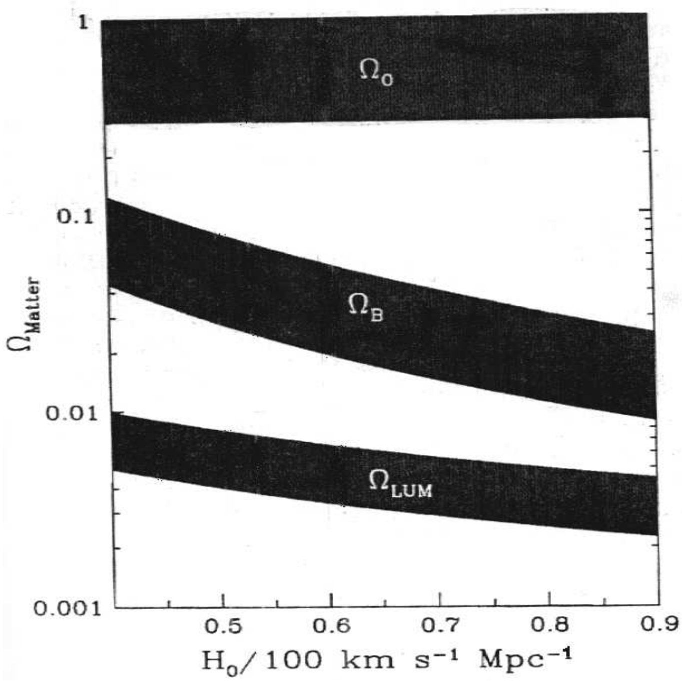

Figure 1.3: Summary of our knowledge about the matter density Ω_M. The lowest band is luminous matter (bright stars and associated materials); the middle one is BBN concordance interval for baryon density. The upper band represents the total matter density based upon dynamical methods. The gaps between the bands illustrate the two dark matter problems: most of the ordinary matter is dark and most of matter is non-baryonic [Schramm & Turner (1998)].

1.1.3 Uncertainties in the determination of baryon density

The procedure to constrain the values of Ω_B, we have described above, has some uncertainties; although many of them have been reduced thanks to improvements both in experimental and theoretical physics (for instance the uncertainty of τ_n, neutron decay period) some still remain important. Here we will focus our attention on few of them:

- errors on observed primordial abundances;
- uncertainty on the Hubble parameter;
- errors on reaction cross section at astrophysical energies.

Up to now, a lot has been done in all these fields, but a definitive solution is still far away from being found.

We will now focus our attention on the lithium case. A crucial problem is the determination of its primordial amount; in order to do this a synergic work between stellar physics and nuclear astrophysics has to be done.

1.2 The primordial Lithium

Observations on halo[5] stars [Spite & Spite (1982)] show a nearly constant lithium abundance for effective temperatures[6], $T_{eff} > 5800$ K in a ε(Li)[7]$\div$ T$_{eff}$ diagram (see figure 1.4). That "Spite Plateau" is taken as a signature of the primordial content of lithium in the Universe. Recent advances [Spite et al. (1996)] indicate that the Spite plateau is exceptionally thin ($\leq$ 0.05). This small dispersion, together with the presence of ^6Li in halo stars [Lemoine et al. (1997), Smith et al. (1993)] seem to suggest that the stellar destruction of ^7Li, if any, is very limited in population II star. The ^6Li isotope is of cosmologic interest as well since, being more fragile than

[5]Halo stars are part of the spheroidal component of our Galaxy and, for their negligible metallic content, are classified among the oldest known stars (Pop. II).

[6]The effective temperature T$_{eff}$ is given, once stellar luminosity and radius are known, by the relation L=$4\pi R^2 \sigma T^4_{eff}$, with σ the Stefan-Boltzmann constant.

[7]The abundance $\varepsilon(X)$ of element X is defined as $\varepsilon(X)$=log N(X)=$log\frac{N_X}{N_H}+12$

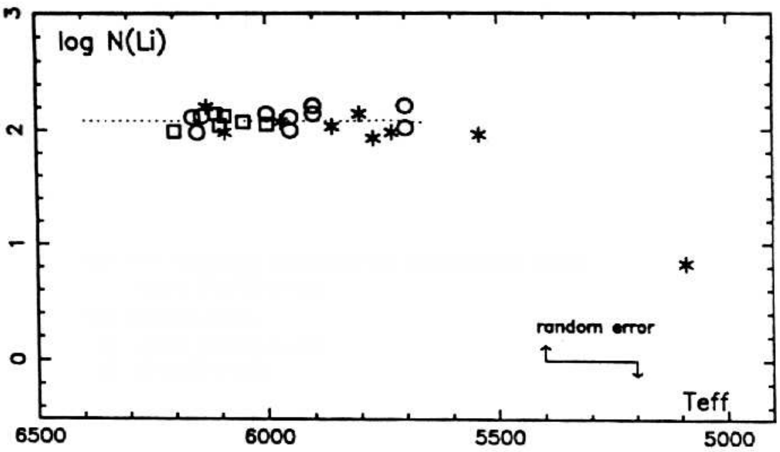

Figure 1.4: The Spite plateau: in a plot of $\varepsilon(Li)$ vs. T_{eff} halo stars, with 5800 $K \leq T_{eff} \leq$ 6400 K, show a nearly constant lithium abundance. The scatter around the mean value ε=2.1 is around 0.08 and is fully explained by experimental errors (see ref. [Spite et al. (1996)]).

^7Li, its mere presence in the atmosphere of halo stars confirms that ^7Li is essentially intact in such stars [Vangioni-Flam et al. (2000)].

However, concerning primordial ^7Li, uncertainty on calculated ^7Li abundance (see fig. 1.2), is still large (up to 30%). One of its main sources can be the reaction rate for $^7Li(p,\alpha)^4He$ which suffers of high errors on low-energy cross section.

But to which extent we can define a lithium abundance to be primordial? In order to do this we have to know how lithium is processed in stars and in galaxies. At a first glance, it is well known that lithium is destroyed during stellar evolution and galactic chemical evolution; in principle older stars must have less content of lithium. But this description is too simplicistic and the phenomenology is more complex, so that a complete stellar model is needed. In table 1.1 we have reported the observed abundances for ^7Li in various astrophysical context.

Theoretical calculations of lithium chemical evolution are still uncertain so the observed abundances may be explained by means of three possible hypotheses:

Astrophysical environment	ε(Li)	reference
Meteorites	3.3	[Anders & Grevesse (1989)]
Sun	1.3	[Anders & Grevesse (1989)]
Population I stars (Hyades)	~ 3	[Thorburn et al. (1993)]
Population I stars (Pleiades)	~ 3.1	[Soderblom et al. (1993)]
Interstellar medium	2.3-2.8	[White et al. (1986), Baade et al. (1991)]
Population II halo stars	2.05-2.22	[Thorburn et al. (1994)]

Table 1.1: Li abundances in various astrophysical environments.

1. BBN has synthesized an amount of ^7Li which corresponds to the "Spite plateau" ($\varepsilon \approx$2.1); Pop I stars are richer in Li because of galactic Li-enrichment and Pop II stars have suffered no significant lithium depletion;
2. BBN has produced the lithium abundance present in the Pop I stars ($\varepsilon \approx$3.1); consequently halo stars have destroyed Li during

   their evolution;
3. the galactic evolution has provided both "lithium factories" and lithium destroying mechanisms.

Until a better understanding of lithium chemical evolution will be achieved, the choice of Spite plateau as a measure of primordial lithium will be an hypotheses, though very reasonable.

1.3 The "Lithium problem"

In order to describe correctly the lithium abundance evolution all the possible producing and depleting mechanisms have to be taken into account in stellar or galactic models. Then the theoretical predictions must agree within experimental errors with available observations, mainly coming from the observation of stellar atmospheres. Even for the best studied star clusters, e.g. the Hyades, lithium depletion is not completely understood [Michaud & Charbonneau (1991)]. Up to now many models have been tested in order to reproduce observative data for open cluster (Hyades or Pleiades) or halo dwarfs [Delyannis et al. (1990)]. This systematic failure of standard models[8] in describing lithium abundances in clusters is referred to as the *"lithium problem"*.

A very useful tool to study lithium abundance in stars is the $N(Li) \div T_{eff}$ plot. In picture 1.5 are reported the Lithium abundance versus T_{eff} trends (the "Lithium morphology") for several galactic clusters of various ages and the Sun as well as for halo stars.

Up to now many efforts have been devoted to study ^7Li abundance in stars; observations of ^6Li in halo stars [Lemoine et al. (1997)] will extend to this isotope the " ^{7}Li problem".

We will now deal with the possible lithium-producing and lithium-depleting mechanisms; we will focus our attention on the latter and in particular on the role of lithium fusion reactions.

Together with cosmological production of lithium, other "factories" had synthetised it. Among them the most important production site for lithium apart from BBN, which has been discussed above, is the interstellar medium, thanks to the spallation reactions on C, O, N nuclides induced by cosmic rays. Naturally it is important to understand how much of the observed lithium was produced in BBN and how much comes out from spallation processes. Current estimates for ^7Li abundance suggest that about a 10% of it has spallation origins [Michaud & Charbonneau (1991)]. For instance ^6Li is almost completely produced by cosmic ray spallation processes.

Mechanisms other than spallation reactions have been suggested as well. Novae,

[8] In stellar physics standard models are spherically symmetric stellar models, with negligible rotation and magnetic fields and where mixing mechanisms other than convection are absent.

Supernovae, Asymptotic Giant Branch stars have been considered as possible sources of lithium isotopes (see [Michaud & Charbonneau (1991)] for a review).

As regards lithium destruction we will focus our attention on the stellar case. Li burning in stellar environments, mainly through the $^7Li+p \rightarrow \alpha+\alpha$ reaction, begins to be important at a temperature around 2.1×10^6 K. If stellar atmosphere (where T$\sim 10^4$ K) had been static, lithium present in the most external layers (the one that is detected by means of stellar spectroscopy) would have been the primordial one, being at temperatures lower than its burning one. Thus understanding mechanisms which deplete lithium is tightly connected to the description of lithium transportation from stellar surface inward and vice-versa. It is known that convective mixing and elements' diffusion can bring lithium at the bottom of the convective envelope where temperatures may be high enough to destroy lithium according to different stellar masses, evolutionary stages and chemical composition.

Convective mixing, which plays a key role in lithium depletion is for instance less efficient in Pop. II stars (due to smaller opacity of their envelope). For this reason many authors have thought of the "Spite plateau" in halo stars (see fig. 1.4), as a direct information on primordial lithium abundance [Spite & Spite (1982)].

However uncovering the meaning of the Spite plateau requires an account of Li depletion in any solar-like star. Without a good description about how the Sun and Pop. I clusters, which are better studied, have depleted Li we cannot hope to predict whether or not Li depletion is expected in halo stars.

1.4 Stellar models

We will now review few standard stellar models for Pop I stars, which are the best studied ones both theoretically and experimentally. We will then focus our attention on the open problems.

1.4.1 Pre-Main-Sequence

Stars are totally convective during the beginning of their life (Pre-Main-Sequence phase, PMS) [Kippenhahn & Weigert (1990)] and central temperatures are lower than that required to start the nuclear burning. As far as the star evolves if contracts, thus increasing its temperature and starting to build up a radiative core. If temperature at the bottom of convective zone, T_b is lower than 2.1×10^6 K surface lithium cannot be burned; otherwise is if $T_b \geq 2.1\times10^6$ K lithium abundance on stellar surface will decrease before the star reaches the Main Sequence.

Massive stars (M$\geq$1.4$M_\odot$) have an outer convective envelope in PMS which moves fast outward; for this reason no significant depletion is expected on surface, although lithium is burned at the very center of the proto-star. Less massive stars have a deep convective zone which causes a PMS Li depletion. Many examples of very young objects (Pleiades, $\tau \approx 7\cdot10^7$ years) are known, and observative evidences confirm these predictions.

Moreover these phases are very sensitive to different input parameters of the stellar model: efficiency of external convection, equation of state (which influences the depth of the convective envelope), and opacity. Thus changes in these parameters within known variability ranges can help to reproduce the observations; it seems more difficult to reproduce observations for different stellar objects using the same input parameters.

In figure 1.6 observed abundances for Pleiades and α Persei are compared with different theoretical models.

1.4.2 Main sequence

Low-mass Main Sequence (MS) stars are characterized by a convective envelope which deepens as the stellar mass decreases. As for PMS stars, if $T_b \leq 2.1\times10^6$ K and no extra-mixing is present, the lithium abundance remains constant to the value of the protostar nebula. For G and F[9] MS stars some observations are far to be fully understood: Li abundance for G stars (e.g. the Sun) and F stars (e.g. the so-called "lithium dip[10]" in open clusters) are not correctly described by present-day stellar models.

Pre-Ms and Ms Li depletion may also occur as a result of rotation in both Pop. I and Pop. II stars [Pinsonneault et al. (1992)]. It must be stressed that rotational models predict a small but observable Li abundance dispersion in halo stars, even in the limit of identical age, mass and initial composition; observational evidence seems to attribute the scatter of Spite plateau around a mean value as mostly due to experimental errors [Spite et al. (1996)].

1.4.3 Open questions

The main uncertainties on the description of lithium depletion in population I stars (and in population II, of course) in present-day models are the following:

1. opacities and equation of state used as input data for stellar evolution models;
2. lack of a quantitative description for the external stellar convection;
3. lack of a quantitative description for elements' diffusion in stellar atmospheres;
4. the role of rotation and magnetic fields;
5. indetermination on the $^7Li(p,\alpha)^4He$ reaction cross-section at astrophysical energies.

In particular we note how a better determination of $^7Li(p,\alpha)^4He$ reaction cross section can give stellar models more confidence in lithium depletion predictions and

[9] According to the standard astronomical notation stars with $6000\ K \leq T_{eff} \leq 7500\ K$ are commonly referred to as F stars while stars with $5400\ K \leq T_{eff} \leq 6000\ K$ are called G stars [Cester (1984)].

[10] The low Li abundance for Pop I stars around T_{eff}=6700 K is usually referred to as "lithium dip".

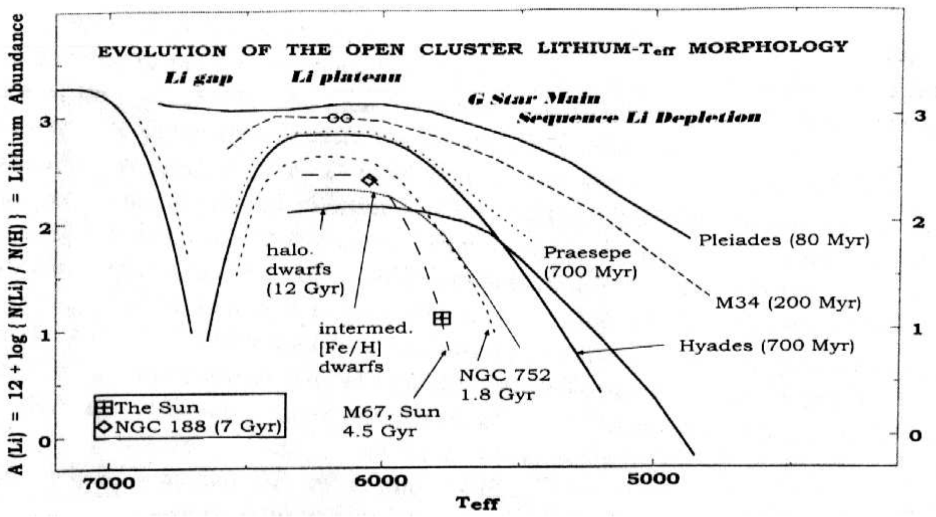

Figure 1.5: Lithium abundance versus T_{eff} trends for some open clusters, as well as for halo dwarfs and the Sun. The most common features of these plots are also indicated (observative data taken from [Michaud & Charbonneau (1991)]).

hence hints on which primordial value for lithium has to be adopted. Moreover its determination is also important for the primordial nucleosynthesis as we have explained in section 1.4.

From the discussions above we can see how nuclear reactions involving lithium at astrophysical energies are important for nuclear astrophysics, cosmology and stellar evolution. We present in this thesis the experimental study of $^6Li(d,\alpha)^4He$ and $^7Li(p,\alpha)^4He$ reactions by using the Trojan Horse indirect method, at the energies relevant for astrophysics. The obtained results will be compared with the presently available ones and the astrophysical implications will be evaluated.

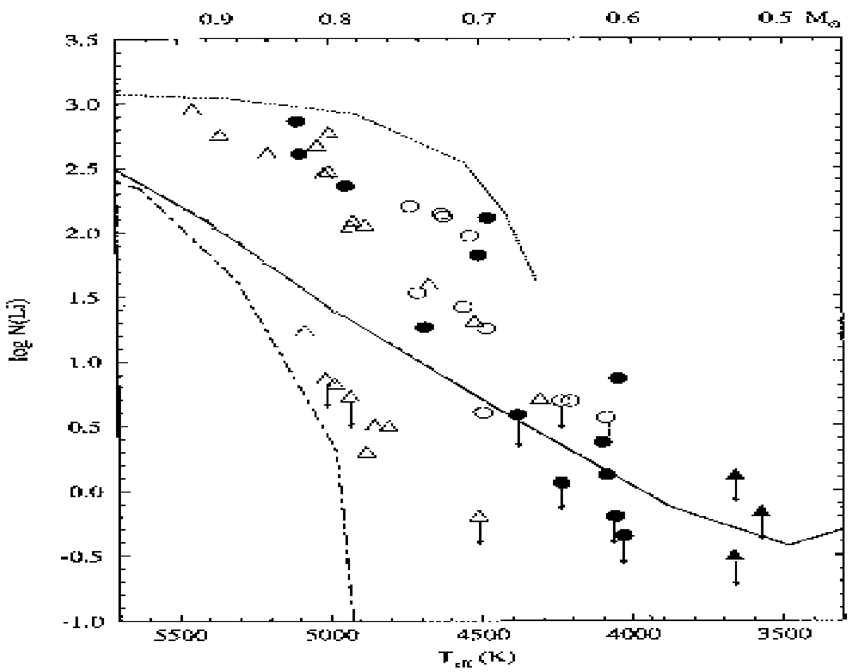

Figure 1.6: Li abundances versus effective temperature and stellar masses for Pleiades (circles) and α Persei stars (triangles), compared with theoretical models. The adopted models are: [Pinsonneault et al. (1990)] (solid and dashed lines, respectively for 0.5 and 1 $\times 10^8$ years) and [D'Antona & Mazzitelli (1994)] (dashed-dotted line).

Chapter 2

The electron screening effect in Nuclear Astrophysics

Experimental and theoretical problems for cross section determinations at energies relevant for astrophysics are presented in the following chapter. Attention will be focused on the electron screening effect and its importance in nuclear astrophysics.

2.1 Cross sections at astrophysical energies

Nuclear reactions play a main role in many astrophysical environments; usually their cross sections are relevant input physical parameters for many astrophysical models. In the Universe, particles may interact by means of their thermal mean energy[1] (which is of the order of few keV). Nuclear reaction between charged particles at such low energies are strongly suppressed by the presence of the Coulomb Barrier whose height (~MeV) is given, in CGS units by:

$$E_C = \frac{Z_1 Z_2 e^2}{R_n}$$

[1]In many astrophysical contexts particles can be described simply by a Maxwell-Boltzmann energy distribution with mean energy $E_m \sim k_B T$.

with R_n the nuclear interaction radius, Z_1 and Z_2 the atomic numbers of the two incident nuclei. Classically, only particles with energies higher than E_c (the extreme high energy tail of the Maxwell-Boltzmann distribution) may interact.

2.1.1 The penetrability factor

According to the quantum mechanics, a particle has a finite probability to penetrate a barrier even if its energy is lower than the barrier's height [Clayton (1983)]. We may define the penetration factor through the Coulomb barrier as

$$T_l = \frac{|\chi(R_n)|^2}{|\chi(R_c)|^2} \tag{2.1}$$

where R_n is the interaction radius, R_c the classical turning point and $\chi(r)$ is the radial wave function. In this way the penetration factor represents the ratio between the probability of finding the incident particle at R_n and that of finding it at R_c

We can calculate it by solving the radial part of the Schrödinger equation:

$$\frac{d^2\chi_l}{dr^2} + \frac{2\mu}{\hbar^2}[E - V_l(r)]\chi_l(r) = 0$$

with

$$V = \frac{l(l+1)\hbar^2}{2\mu r^2} + \frac{Z_1 Z_2 e^2}{r}$$

that is the potential for the l-th partial wave. It may be shown [Clayton (1983)] that T_l can be expressed in terms of the Coulomb regular and irregular functions ($F_l(R)$ and $G_l(R)$)as:

$$T_l = \frac{1}{F_l^2(R) + G_l^2(R)} \tag{2.2}$$

This expression can be approximated, for R=0 and l=0, giving the so-called Gamow factor

$$T = e^{-2\pi\eta}$$

with the Sommerfeld parameter, $\eta = Z_1 Z_2 e^2/\hbar v$, depending only on the relative velocity of the two interacting particles and their charges.

2.1.2 Reaction rate and the Gamow peak

The reaction rate is defined as the number of reaction a(A,b)B per unit volume per unit time and is written in terms of the cross section σ as:

$$r_{aA} = \frac{1}{1+\delta_{aA}} n_a n_A < \sigma v > \tag{2.3}$$

where δ_{aA} is the Kronecker symbol and $< \sigma v >$ is the mean of the product σv over all the possible energies, weighted over the Maxwell-Boltzmann distribution

$$r_{aA} = \frac{1}{1+\delta_{aA}} n_a n_A \int_0^\infty v\sigma(v)\phi(v)dv$$

being n_a and n_A the number densities of particles a and A respectively.

The maximum of the integrand is reached at energy E_0:

$$E_0 = \left(\frac{bk_bT}{2}\right)^{\frac{2}{3}} = 1.22(Z_a^2 Z_A^2 \mu T_6^2)^{\frac{1}{3}} \qquad keV$$

with $b = (2\mu)^{\frac{1}{2}}\pi e^2 Z_a Z_A/\hbar$ and $T_6 = T/10^6$ K. This energy correspond to the so-called **Gamow peak** and represents the most effective energy for thermonuclear reactions; usually it ranges from few keV to few hundred keV depending on both the reaction and the astrophysical site in which the reaction takes place. As we can see from picture 2.1 the Gamow peak has a finite width, which is referred to as the Gamow window [Rolfs & Rodney (1988)]. We also note that the energy corresponding to k_BT is lower than the centroid of the Gamow peak.

2.2 Direct measurements at astrophysical energies

In spite of the tunnel effect, the Coulomb barrier plays a key role in reducing the cross-section at energies around E_0. Usually at energies corresponding to the Gamow peak, cross section is less than few nanobarns (see [Rolfs & Rodney (1988)] for some experimental examples). In such conditions, experimental measurements of cross

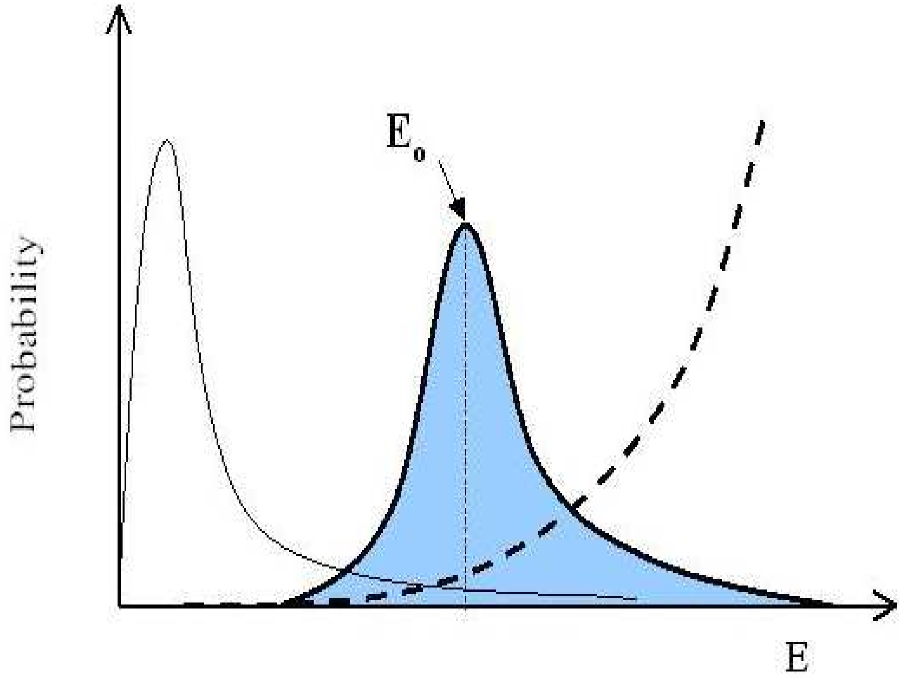

Figure 2.1: The convolution of the Maxwell-Boltzmann distribution and the penetrability factor defines the Gamow Peak, which is amplified in this picture. Its corresponding energy is E_0.

section are a hard task. The number of detected particles in one second, N_d depends on the cross section σ through:

$$N_d \propto \sigma \; N_i \; \tau \; \Delta\Omega \tag{2.4}$$

where τ is the target thickness, $\Delta\Omega$ the solid angle covered by the detector and N_i the number of incident particles per second.

Maintaining a constant $\Delta\Omega$, N_d may be increased by using more intense beam currents or thicker target. But an increase on the beam current would cause an excessive target heating due to beam-energy dissipation; so gas targets have been used, thus affecting the definition of the effective target-thickness. Moreover not every element can be put in a gas target and damages for the detectors, in case of high beam current would be serious. Additionally a rather thick target will imply a worse energy resolution.

Even if the number of detected particles (the "signal") might increase by improving experimental skill, the "signal to noise" ratio can be, for nuclear astrophysics experiments, so low (at lower energies) that no significant measure can be done.

Possible sources of noise can come from the cosmic and natural radiation background, from the electronic devices used, etc. Different ways have been suggested in order to bypass this problem:

- the use of very low-radiating devices and very low-noise electronics;
- to perform nuclear astrophysics experiments in low-noise environments, as the Laboratori Nazionali del Gran Sasso;
- the use of different kinds of indirect methods.

For these reasons, with the exception of few cases (e.g. [Bonetti et al. (1999)]), in order to measure nuclear cross sections at astrophysical energies one needs to extrapolate the cross section's trend at lower energies. This is usually done by defining the astrophysical S(E) factor.

2.2.1 The astrophysical S(E) factor

For charged particle nuclear reaction it is possible to factorize the cross section as:

$$\sigma = \frac{1}{E} S(E) e^{-2\pi\eta} \tag{2.5}$$

where η is the Sommerfeld parameter. The first term takes into account the wave properties of quantum particles, $e^{-2\pi\eta}$ represents a rough approximation of the Coulomb penetration factor, while S(E) is defined as the astrophysical factor. It shows for many reactions a slight dependence on the energy (especially in comparison with the low energy cross section behaviour, see figure 2.2); this allows an easier procedure for extrapolating the energy behaviour at astrophysical energies. If we

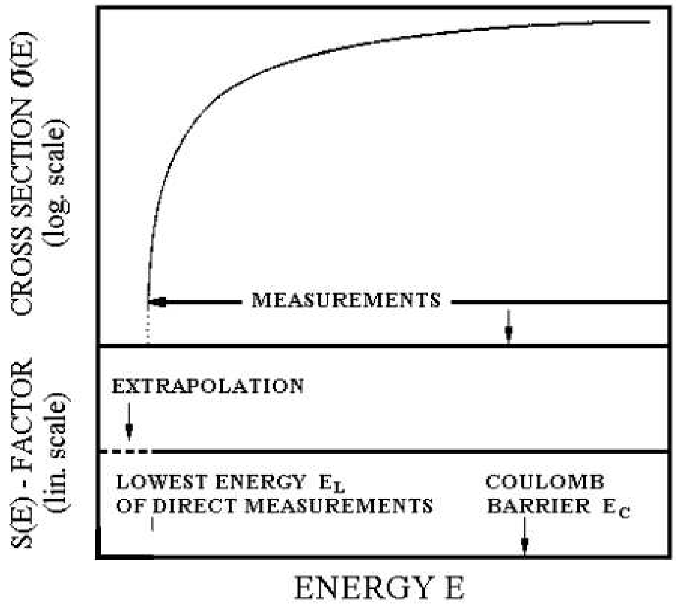

Figure 2.2: Comparison between the energy behavior for cross section and astrophysical factor. While the cross section has a dramatical energy-dependence the astrophysical factor is practically constant.

substitute the definition of the S(E) factor in eq. 2.3 we obtain:

$$r_{aA} = \frac{1}{1+\delta_{aA}} n_a n_A \sqrt{\frac{8}{\pi\mu}} (k_b T)^{-\frac{3}{2}} \int_0^\infty S(E) exp \left[-\frac{E}{k_b T} - \frac{b}{\sqrt{E}} \right] dE$$

Extrapolation down to astrophysical energies is usually done by means of the S-factor; the standard procedure consists in fitting the high energy data using an appropriate theoretical function (in the simplest approximation a polynomial). Then this is extrapolated to the astrophysical energies.

Anyway, the presence of low energy or sub-threshold resonances [Rolfs & Rodney (1988)] and electron screening makes the extrapolation less reliable. In particular the contribute of sub-threshold resonances to the astrophysical factor can be dominant at astrophysical energies; for this reason their presence must be taken into account in the extrapolations (see figure 2.3).

We will deal with the electron screening effect in the next section.

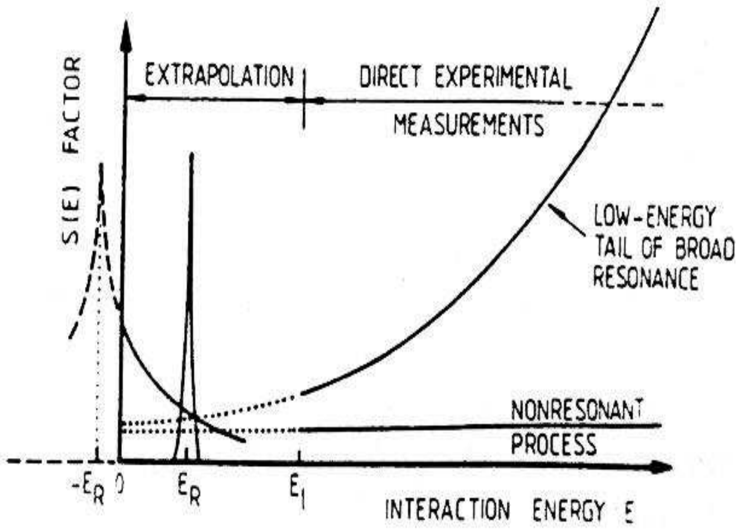

Figure 2.3: S(E)-factor in the case of a sub-threshold resonance at energy -E$_R$; the contribution of a broad and a narrow resonance are also sketched. The extrapolation without taking into account the resonances represents only a lower limit of the S(E)-factor.

2.3 The electron screening effect

Up to now we have considered the interacting nuclei as completely stripped of electrons. In this way the Coulomb potential has an infinite range and takes the form:

$$V_C = \frac{Z_1 Z_2 e^2}{r} \tag{2.6}$$

with Z_1 and Z_2 the interacting nuclei charges, r the relative distance and e the electron charge. This holds for "bare nuclei". But for nuclear reactions studied in the laboratory, target and projectile nuclei are always bound in neutral atoms or molecules and ions. The interaction between nuclides and their electron clouds will cause the phenomenon referred to as the *electron screening effect* [Assenbaum et al. (1987)], which produces an enhancement of the "bare" S(E) factor at low energies by a factor [Engstler et al. (1992)]:

$$f(E) = \frac{S_s}{S_b} = \frac{E}{E+U_e} e^{\left(\frac{\pi\eta U_e}{E}\right)} \approx e^{\left(\frac{\pi\eta U_e}{E}\right)}$$

where S_s and S_b are the shielded and the bare nucleus S-factor, respectively. We will briefly explain the theoretical basis of this result in section 2.4. The expected enhancement has been observed in several fusion reactions ([Engstler et al. (1992)] and references therein) and has been studied both theoretically and experimentally for various reactions. This effect is shown in figure 2.4 for the $^7Li(p,\alpha)^4He$ reaction.

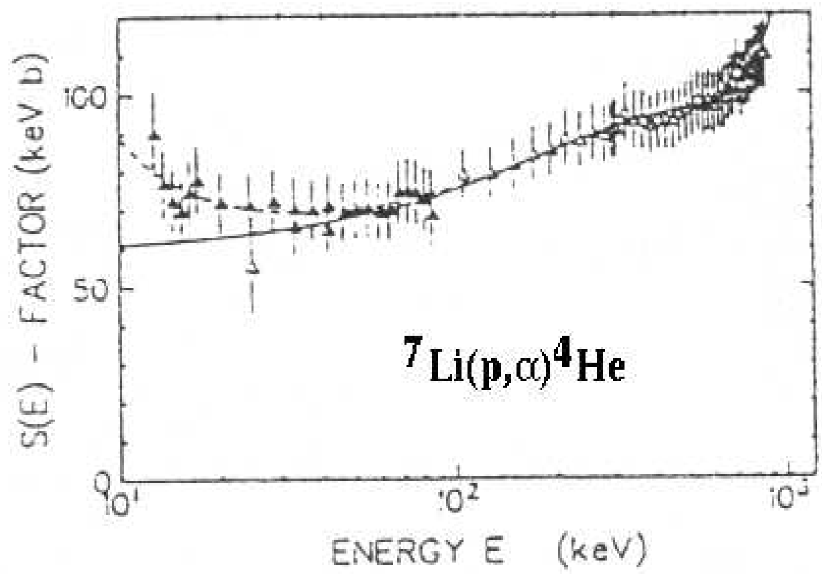

Figure 2.4: The S(E) factor for the $^7Li(p,\alpha)^4He$ reaction. The enhancement at very low energies is visible [Engstler et al. (1992)].

It has been seen that the lower the interaction energy the larger this enhancing factor is. In the next section we will see that what is needed for astrophysics is the bare nucleus astrophysical S(E)-factor, S_b(E), and again, even if direct measurements are available in the Gamow window, extrapolations are needed in order to extract it from direct measurements by using

$$S_b = S_s \cdot e^{\left(-\frac{\pi\eta U_e}{E}\right)} \tag{2.7}$$

where $S_s(E)$ is the measured (and shielded) S-factor.

2.3.1 Electron screening in stellar environment

For the high temperatures occurring in stars, atoms are generally completely stripped of their electron clouds and one can imagine that electron screening has no effect on nuclear reactions in stars. However nuclei are embedded in a sea of free electrons, whose final effect is similar to the one discussed above, since free electrons tend to cluster in the area surrounding a nucleus.

If k_BT is larger than the electrostatic energy between the particles, a stellar gas is called "nearly perfect". In this case it can be shown [Clayton (1983), Rolfs & Rodney (1988)] that electrons tend to cluster into spherical shells around a nucleus at the Debye-Hückel radius R_D

$$R_D = \left(\frac{k_BT}{4\pi e^2 \rho N_A \xi}\right)^{1/2}$$

where N_A is the Avogadro's number and $\xi = \sum_i (Z_i^2 + Z_i)\frac{X_i}{A_i}$, the sum being over all positive ions and X_i the mass fraction of the i^{th}-nucleus of charge Z_i.

As for the laboratory, electron screening in stars enhances the charged particles cross section and the thermonuclear reaction rates of a stellar enhancing factor $f^*(E)$, according to the equation:

$$< \sigma v >_{s*} = f^*(E) \cdot < \sigma v >_b \tag{2.8}$$

This is, in general, different from the screening factor in the laboratory. It has to be stressed that in order to have an astrophysically relevant information, the bare nucleus reaction rate (hence the bare nucleus astrophysical factor) has to be known.

Thus it is necessary to know the electron screening factor in the laboratory in order to extract the bare nucleus S(E)-factor from the shielded one (eq 2.7). Then the appropriate stellar screening factor (eq. 2.8) should be applied to that. Moreover, understanding electron screening in the laboratory will give hints on stellar electron screening and its theoretical description.

2.4 Theoretical description of the electron screening effect

The first descriptions of the electron screening effect and the first theoretical estimates of the screening potential U_e are based on the *Born-Oppenheimer* approximation. The assumption is that electronic degrees of freedom are well separated from the nuclear ones, and that they are negligible as well. Models like these are very simple since they don't take into account the fact that spatial electronic distribution can change during the collision of nuclei.

In such a simple model when a particle hits on a target nucleus, it has to penetrate the effective Coulomb barrier that can be defined as the difference between the bare nucleus Coulomb barrier and the screening potential (see figure 2.5):

$$V_{eff} = V_{Coul}(r) - V_{scr}(r) = \frac{Z_1 Z_2 e^2}{r} - V_{scr} \tag{2.9}$$

in a standard notation.

In this contest the penetration through a shielded Coulomb barrier at projectile energy E is equivalent to that of bare nuclei at energy $E_{eff} = E + U_e$

By solving the Schrödinger equation in WKB (Wentzel-Kramers-Brillouin), see [Satchler (1990)], approximation it is possible to express [Assenbaum et al. (1987)] the enhancing screening factor in terms of:

$$f(e) = \frac{\sigma(E_{eff})}{\sigma(E)} = (E/E_{eff}) \left(\frac{exp - 2\pi\eta(E_{eff})}{exp - 2\pi\eta(E)} \right) \approx exp\left(\pi\eta\frac{U_e}{E}\right) \tag{2.10}$$

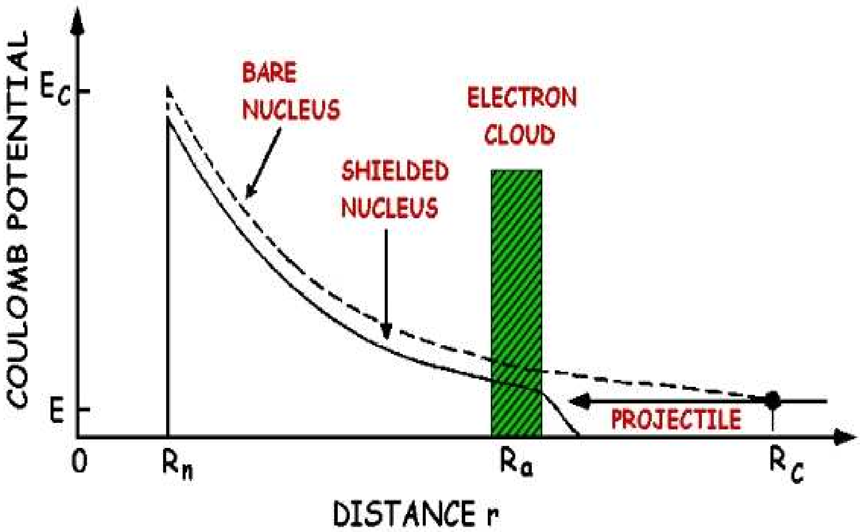

Figure 2.5: Coulomb potential modified by the presence of orbital electrons (shielded nucleus); the dashed line shows the shape of the bare nucleus potential.

where it has been used the approximation $E_{eff} \sim E$.

For energies $E/U_e \geq 1000$ it has been shown shielding effects are negligible [Assenbaum et al. (1987)]; thus above these energies the bare nucleus cross section may be measured directly in the laboratory. At energies $E/U_e \leq 100$, screening effects cannot be disregarded in direct measurements and one essentially measures a shielded cross section.

The value of the potential U_e is usually estimated from approximate theoretical models that we will review in the next section. It can also be experimentally measured from direct measurements or by using indirect methods; we will later deal with the problems connected with the experimental determination of U_e.

We will now examine few simplified descriptions of the screening effect [Bluge (1989)]; each one of these models provides an evaluation of the screening potential U_e. For simplicity's sake it is assumed that the projectile nucleus is completely ionized while the target nucleus has Z electrons.

Rolfs's model

In this model one assumes a surface distribution for the electronic charge, at a distance r_a, with r_a the radius of the innermost electrons of the target nucleus. Hence, for $r > r_a$ the potential acting on an incident particle is zero because of atom's neutrality, while for $r < r_a$ the barrier is reduced by the presence of electron cloud (see fig. 2.5). So for the potential U_e it is assumed [Bluge (1989)] that:

$$U_e = \frac{Z_1 Z_2 e^2}{r_a}$$

where Z_1, Z_2 are the nuclear charges of projectile and target respectively.

Bencze's model

Bencze obtains, within the static approximation[2], for U_e the value [Bencze (1989)]:

$$U_e = \frac{3Z_1 Z_2 e^2}{2r_a}$$

where r_a, the screening radius, has a numerical value of:

$$r_a = 0.8853 a_0 (Z_1^{2/3} + Z_2^{2/3})^{-1/2}$$

extracted from the atomic scattering studies by [Lindhar (1968)] and where a_0 denotes the Bohr radius. In this model the nuclear radius is considered nearly zero and the electron charge is uniformally distributed in a spherical volume of radius r_a.

2.4.1 Adiabatic and sudden approximation

Models described previously do not take into account the fact that, during the collision, changes of the electronic charge distribution may occur. Thus models that include a dynamical description of the process are needed. This could be one of

[2]The static approximation assumes an *a priori* electron distribution; within this hypothesis the variation of electronic spatial distribution during the collision is not taken into account.

the reasons why predictions for U_e, made through theoretical models based on the Born-Oppenheimer approximation, are sensibly different from values extracted from experiments (see next section).

For simplicity's sake we will distinguish two opposite cases: the low-velocity case (or adiabatic approximation) and the high-velocity case (sudden approximation).

Adiabatic approximation (low velocity case)

When the motion of the nuclei is much slower than that of the electrons, during the collision the electron wave function re-adjusts itself so that at any time it is an eigenfunction of the two-center Hamiltonian. So it is possible to establish a correspondence between the separate and the compound atoms wave functions, which determines (see [Bracci et al. (1990)]) the energy transfer U_{ad}. It can be shown [Bracci et al. (1990)] that in this approximation the screening potential U_{ad} is simply:

$$U_{ad} = E^{(1)} + E^{(2)} - E^{(c)}$$

where $E^{(1)}$ is the electronic binding energy for the first atom, $E^{(2)}$ the second atom's one and $E^{(c)}$ the electronic binding energy for the compound atom.

Sudden approximation (high velocity case)

The case when the relative velocity of nuclei is much larger than the electrons' one can be discussed by using the sudden approximation, i.e. the electron distribution at fusion time is almost the same as it was in the initial state. It can be shown that the electron energy variation between the initial configuration and the fusion time is simply due to the variation of the electronic potential energy once the nucleus Z_1 is replaced by the compound nucleus $Z_1 + Z_2$, the electronic wave function being unaffected [Bracci et al. (1990)]. The energy fraction transferred to the relative nuclear motion is found to be:

$$U_{sud} =< \phi^{(1)}| \sum_i \frac{Z_2^2 e^2}{r_i} |\phi^{(1)} > \left[1 - \frac{M_2}{M_1 + M_2}\right]$$

Target	Projectile	U_a (eV)	U_s (eV)	Target	Projectile	U_a (eV)	U_s (eV)
H	p	20.4	13.6	^7Li	p	186	134
H	d	20.4	9.1	^3He	d	119	54

Table 2.1: Adiabatic and sudden approximation results for some reactions of astrophysical interest (taken from [Bracci et al. (1990)]).

the sum being over the electrons of the target atom, r_i is the distance of the ith electron from the compound nucleus and $|\phi^{(1)} >$ the initial state.

In table 2.1 some results for different reactions are reported for both the approximations. Other dynamical models have been worked out, some of them using the Time Dependent Hartree Fock (TDHF) method (see for example [Shoppa et al. (1993)]). In figure 2.6 the trend of U_e versus energy is plotted for the ^3He+d reaction: we remark that at $E \sim 0$ the TDHF is consistent with the adiabatic approximation as well as with the sudden approximation at higher energies.

2.5 Experimental determination of the screening effect

Experimental determinations of the screening potential U_e have been performed for a large number of astrophysically relevant reactions. The extracted value has been compared with that calculated by theory, usually through the adiabatic approximation which is valid for astrophysical energies.

The procedure for extracting the potential U_e from low-energy data is the following [Fiorentini et al. (1995)]:

1. high energy experimental data at $E/U_e \geq 1000$, where the effects of electron screening are negligible, are analyzed using polynomial fits or, if available, nuclear reaction models in order to obtain an analytic expression for $S_b(E)$;

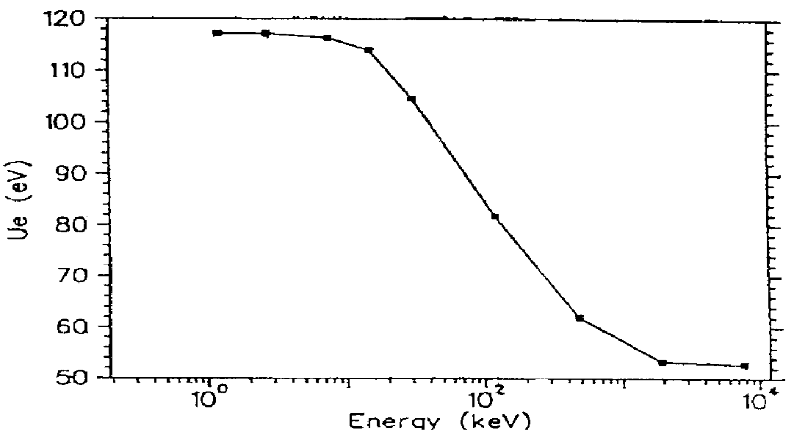

Figure 2.6: Trend of U_e versus energy for the $^3He(d,p)^4He$ reaction according to [Shoppa et al. (1993)]. We remark that at energies around zero it is consistent with the adiabatic value U_e=119 eV while at higher energies it agrees with the sudden approximation, U_e=54 eV.

2. the derived $S_b(E)$ factor for bare nuclides is then extrapolated into the energetic region where electron screening effects are expected;

3. the experimental shielded $S_s(E)$-factor, at energies such that $E/U_e \leq 100$,are used together with equation 2.7 to fit data with U_e as the only fit parameter.

It's easy to understand that the extracted values for U_e are sensitively dependent on the assumed (and extrapolated) $S_b(E)$. So even if a measurement is performed at astrophysical energies, extrapolations are needed in order to correct the S(E) factor for the electron screening. Independent information on the bare nucleus cross section would be needed for many charged-particle reactions indeed.

2.5.1 Applications

The method presented above has been applied to many reactions. Many experimental efforts have been devoted to the determination of the screening potential; we will briefly discuss the results obtained for lithium-depleting reactions [Engstler et al. (1992)] and for the $^3He(d,p)^4He$ reaction [Costantini et al. (2000)].

In figure 2.7 and 2.8 experimental data for $^6Li(d,\alpha)^4He$ and $^7Li(p,\alpha)^4He$ and $^3He(d,p)^4He$ are respectively reported. The extrapolated bare-nucleus astrophysical factor (solid lines), $S_b(E)$, and the fit including screening effects (dashed lines) are plotted. The extracted screening potentials are compared to the predictions of the adiabatic approximation in table 2.2. A systematic discrepancy can be observed for U_e for these three reactions; its explanations are currently under investigation.

In particular the possible solution can be found in one (or more) of these still open research fields:

- Atomic physics: presently available models disagree with the experimental determination. Are the adopted theoretical approaches and approximations correct?

- A possible error-source for experimental data can be the extrapolation of energy loss at astrophysical energies. Direct measurements of energy loss at very low energies can help in obtaining a better estimate of the shielded S(E)-factor and thus of U_e [Langanke et al. (1996)];

- extrapolations from high energy experimental data to obtain the bare astrophysical factor at very low energies, can introduce large uncertainties on the fitted value of U_e; an independent method to measure $S_b(E)$ is needed indeed.

In this thesis we present the Trojan Horse Method (THM) as a complementary tool to obtain independent information on bare nucleus cross section. We will apply this method to measure the bare nucleus astrophysical factor for $^6Li(d,\alpha)^4He$ and $^7Li(p,\alpha)^4He$ reactions and hence the screening potential.

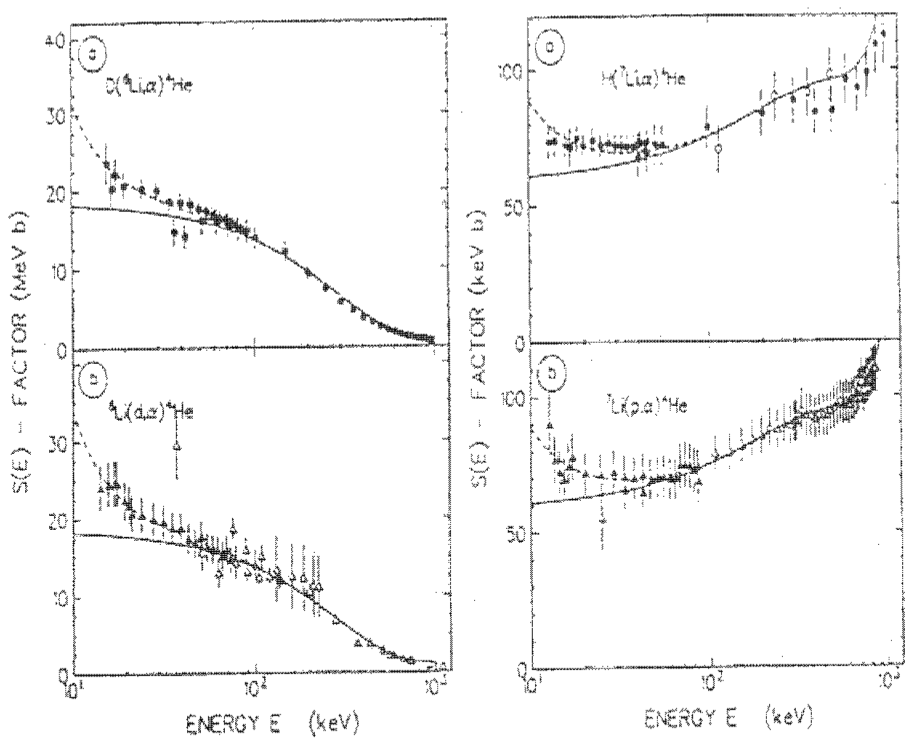

Figure 2.7: The S(E) factor for ${}^6Li(d,\alpha)^4He$ and ${}^7Li(p,\alpha)^4He$ in direct and inverse kinematic [Engstler et al. (1992)]. The fit to determine the screening potential is also shown together with the bare nucleus S_b(E)-factor; data are obtained through the use of (a) molecular hydrogen targets and (b) LiF solid targets (see text for further details).

2.6 Electron screening effect and Lithium depletion

As it is reported in [Castellani et al. (1996)] the value of the screening potential for the ${}^7Li + p \rightarrow \alpha + \alpha$ may play a crucial role for the explanation of lithium abundances in the atmosphere of solar-type stars (see chapter one). At the bottom of the convective zone, physical conditions (in particular the inter-particle distance and the electron velocity) are very similar to the ones of laboratory electrons. So,

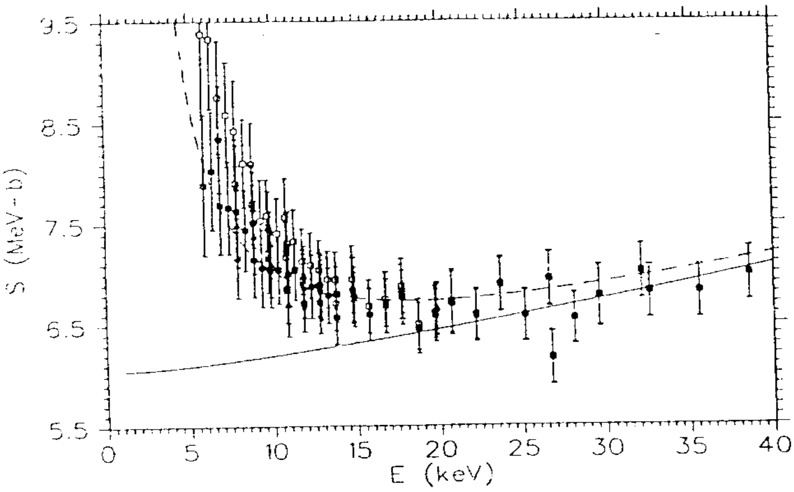

Figure 2.8: S(E) factor for the $^3He(d,p)^4He$ reaction. A comparison is made between data obtained using standard energy-loss (open dots) and data from [Langanke et al. (1996)] (full dots). The dashed line represents the shielded nucleus fit and the solid one the bare nucleus contribution.

at a first approximation it is possible to assume that $U_{e*}^{p+Li} \sim U_{lab}^{p+Li}$, i.e. that the stellar screening potential is similar to the laboratory one.

Under these assumption it can be shown [Castellani et al. (1996)] that the nuclear burning rate for lithium is:

$$< \lambda_{pl}^{p+Li} > \propto \rho_b X_b T_b^{\alpha} exp\left(\frac{U_{e*}^{p+Li}}{k_B T_b}\right) \tag{2.11}$$

with ρ_b, T_b, X_b, the density, the temperature and the hydrogen mass fraction at the bottom of convective zone for a star of solar mass, while the exponent is $\alpha \approx 19.7$ for the $^7Li + p \rightarrow \alpha + \alpha$ reaction.

It has been seen [Castellani et al. (1996)] that a value of U_{e*}=600÷700 eV fits the observational data for the Hyades [Thorburn et al. (1993)] (see fig. 2.9) for stars with $T_{eff} \leq 6400$ K. This value can be compared with U_e=300 eV of experimental determination [Engstler et al. (1992)] and U_e=186 eV of the adiabatic approxima-

Target	Projectile	U_{ad} (eV)	U_{exp} (eV)
^7Li	p	186	300±280
^6Li	d	186	380±250
^3He	d	119	130±9

Table 2.2: Comparison between the calculated screening potential for adiabatic approximation and the experimentally extracted one [Engstler et al. (1992), Costantini et al. (2000)]. See text for more details.

tion.

It appears again necessary to perform an independent measurement for U_e for the $^7Li + p \rightarrow \alpha + \alpha$; this was done, as well as for the $^6Li + d \rightarrow \alpha + \alpha$ reaction, by applying the indirect method of the Trojan Horse (THM).

The next section will deal with the bases of the THM and the theoretical formalism which is necessary for extracting the bare astrophysical factor for the studied reactions.

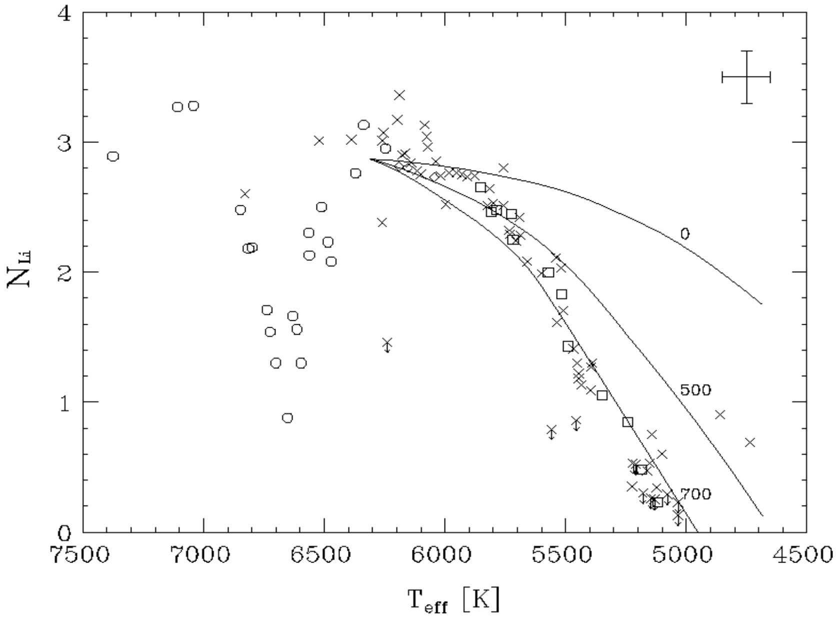

Figure 2.9: Li abundance data for the Hyades dwarfs as a function of the effective temperature. The curves represents calculation for various values of U_{e*} (eV) [Castellani et al. (1996)].

Chapter 3

The Trojan Horse Method: a complementary tool for Nuclear Astrophysics

Fracti bello fatisque repulsi
ductores Danaum, tot iam labentibus annis,
instar montis equum divina Palladis arte
aedificant, sectaque intexunt abiete costas.
AEN. L. II

As reported in the previous chapter, direct measurements have to face many experimental difficulties as one tries to investigate very low energy regions ($E_{cm} <$ 100 keV). Nevertheless the presence of electron screening effects in the laboratory makes extrapolation necessary at such energies, even if direct measurements are available. The confidence to put in such extrapolation is of course linked to the extension of the unexplored energy region.

For these reason many indirect methods have been proposed; Coulomb dissociation, transfer reactions and inverse reactions are nowadays used whenever it is not possible to study a certain reaction in a direct way (see [Arnould & Takahashi (1999)] for an overview).

In this chapter we will deal with the Trojan Horse Method (THM) which has been proposed in order to by-pass these experimental problems.

3.1 Quasi-free break-up

The "quasi free" reactions are direct three body processes characterized by the presence of a "spectator" particle, s, in the exit channel, i.e. a particle that retains the momentum it had in the initial channel [Satchler (1990)].

Such reactions can be sketched as:

$$A + a \to C + c + s \tag{3.1}$$

If we assume that the nucleus A has a high probability to be composed by two clusters, i.e. $A = x \oplus s$, we can define a "quasi-free break-up" process when, after the break-up of particle A, the cluster s retains the same momentum it had in the nucleus A. This process can be sketched, using a pseudo-Feynman diagram, as reported in figure 3.1.

In this picture the upper pole represents the break-up of nucleus A into x and s while the lower one describes the two-body interaction $a(x, c)C$. Usually the break-up can take place either in the target or in the projectile; in some cases it takes place in both target and projectile nuclei.

3.1.1 Sequential Mechanisms

In order to apply the Trojan Horse Method, which is based on a quasi-free break-up process, one needs to separate this process from all the others which may occur between the same target and projectile, giving the same particles in the exit channel (e.g. the sequential processes). They may be described by means of a two step interaction, in which the final state is reached through an intermediate one, as sketched

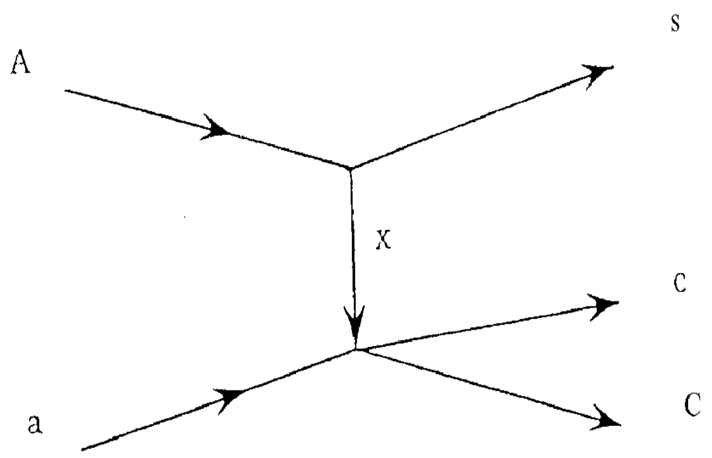

Figure 3.1: A pseudo-Feynman diagram for a quasi-free reaction; the nucleus A is considered as composed of clusters x and s. See text for further details.

in picture 3.2. Although sequential processes are dominant within 3-body reactions, under particular experimental cinematic conditions and in some energy regions, their contribute can be distinguished and separated from the quasi-free one. In particular sequential contribute is, in these cases, "noise" and must be removed during off-line analysis. In picture 3.2 one of the possible sequential processes occurring in the three-body reaction 3.1 is sketched.

3.2 The Trojan Horse Method

The method allows us to derive indirectly the cross section of a two-body reaction of astrophysical interest

$$A + x \to C + c \tag{3.2}$$

from the cross section measurement of a suitable three-body process

$$A + a \to C + c + s \; .$$

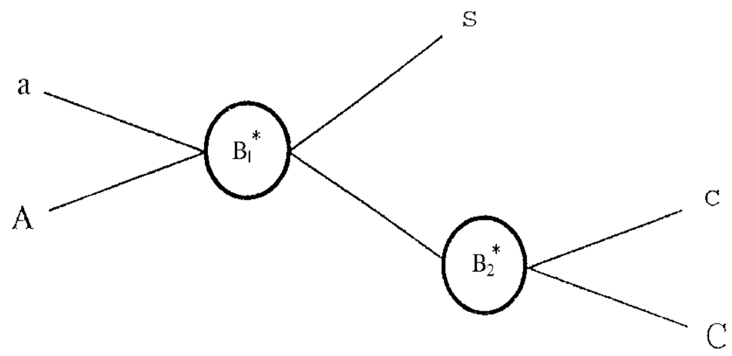

Figure 3.2: A possible 3-body sequential process which gives in the exit channel particles s, c, C through the formation of intermediate nuclei.

It was first proposed by G. Baur [Baur (1986)] as a tool to indirectly investigate at very low energy the cross section of charged particle induced reaction. Following the description reported in the previous section, the nucleus A is considered to be dominantly composed of clusters x and s.

The energy in the entrance channel $A + a$ should be chosen above the height of the Coulomb barrier, so as to avoid the reduction in cross section due to barrier penetration. At the same time the effective energy of the reaction between A and x could be relatively small because the binding energy and the relative motion of x inside A can compensate for the energy in the entrance channel, as it is sketched in figure 3.3.

Since the transferred particle x is hidden inside the nucleus A, which acts like a Trojan Horse, and the collision between a and x takes place in the nuclear interaction region, the two-body reaction cross section is almost free from Coulomb suppression and, at the same time, is not affected by electron screening effects. Moreover the relative energy between A and a may be really small and allows to study the process $A(x, c)C$ at astrophysical energies.

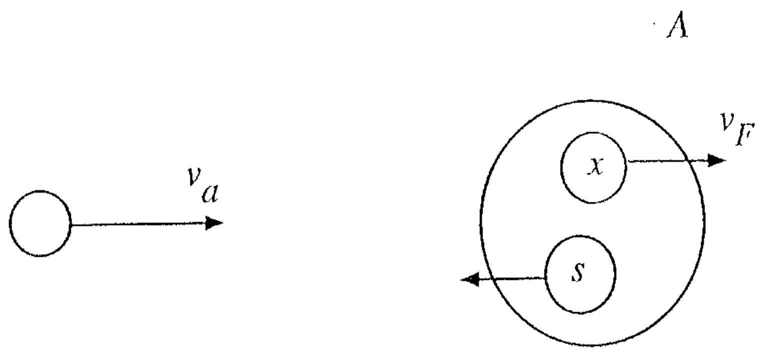

Figure 3.3: The interaction between x and a takes place at very low energy thanks to binding energy and the relative x-s motion inside A.

3.3 Theory

The experimental application of the Trojan Horse Method, has been developed in Catania; as a first approximation the PWIA [Cherubini et al. (1996), Calvi et al. (1997), Spitaleri et al. (1999)] has been adopted as it will be explained in the following section. The more recent formalism in DWIA [Typel & Wolter (2000), Spitaleri et al. (2001)] will be reviewed in section 3.4.2.

3.3.1 Cross section in PWIA

In order to describe the THM theoretically, it is useful to use the Impulse Approximation [Chew & Wick (1952)]. The fundamental hypothesis on which it is based on are:

- the incident particle never interacts strongly with both the constituents of the system A at the same time;
- the amplitude of the incident wave falling on each constituent is nearly the

same as if those were alone;

- the binding energy between s and x inside A is negligible.

In the Plain Wave Impulse Approximation (PWIA) [Satchler (1990)] the three-body differential cross section may be expressed as [Jain et al. (1970)]:

$$\frac{d^3\sigma}{dE_c d\Omega_c d\Omega_C} \propto KF \cdot |g_j(\vec{K}_s)|^2 \cdot \frac{d\sigma_{ax}^N}{d\Omega'} \tag{3.3}$$

where KF is a kinematical factor, $|g_j(\vec{K}_s)|^2$ is the momentum distribution of the spectator s inside A and $d\sigma_{ax}^N/d\Omega'$ is the nuclear differential cross section for the two-body interaction $a + x \to c + C$.

Assuming that $|g_j(\vec{K}_s)|^2$ is known and calculating KF from the experimental and kinematical conditions, is then possible to derive $d\sigma_{ax}^N/d\Omega'$ from the direct measurement of the three-body differential cross section, $d^3\sigma/dE_c d\Omega_c d\Omega_C$. It has to be emphasized that the obtained $d\sigma_{ax}/d\Omega'$ is the nuclear part, the Coulomb barrier being already overcome in the entrance channel according to what we have explained above. So in order to get the "usual" two-body cross section it will be necessary to multiply for the transmission coefficient through the Coulomb barrier:

$$\frac{d\sigma}{d\Omega} = \sum_l G_l \frac{d\sigma_l^N}{d\Omega} \tag{3.4}$$

where G_l represents the transmission coefficient for the l-th partial wave and $\frac{d\sigma_l^N}{d\Omega}$ is its related cross section [Cherubini et al. (1996), Spitaleri et al. (1999)]. This empirical assumption have to be justified; in order to do this and to better elucidate the connection between the three and the two body cross section a new formulation in Distorted Wave Born Approximation (DWBA) has been introduced.

3.3.2 Formulation of THM in DWBA

The three-body differential cross section of the reaction $A + a \to C + c + s$ can be calculated with the help of the DWBA [Typel & Wolter (2000)] and written as

$$\frac{d^3\sigma}{dE_C d\Omega_C d\Omega_c} = KF\, |T_{fi}|^2 \tag{3.5}$$

with a kinematical factor

$$KF = \frac{\mu_{Aa} m_c}{(2\pi)^5 \hbar^7} \frac{p_C p_c^3}{p_{Aa}} \left[\left(\frac{\vec{p}_{Bs}}{\mu_{Bs}} - \frac{\vec{p}_{Cc}}{m_c} \right) \cdot \frac{\vec{p}_c}{p_c} \right]^{-1} \tag{3.6}$$

in standard notation for (relative) momenta and (reduced) masses. The T-matrix element is written as follows

$$T_{fi} = \langle \chi_{Bs}^{(-)} \Psi_{Cc}^{(-)} \phi_b | V_{xs} | \chi_{Aa}^{(+)} \phi_A \phi_a \rangle \tag{3.7}$$

with:

- $\chi_{Bs}^{(-)}$ (where $B = c \oplus C$), $\chi_{Aa}^{(+)}$ distorted waves;
- ϕ_A, ϕ_a, ϕ_s wave functions of the nuclei A, a and s, respectively;
- $\Psi_{Cc}^{(-)}$ the full two-body scattering wave function;
- V_{xs} he interaction between the transferred particle x and the spectator s.

Using the so-called "surface approximation[1]" (see [Typel & Wolter (2000)]) and the plane wave approximation for the distorted waves, the three-body differential cross section assumes the form

$$\frac{d^3\sigma}{dE_C d\Omega_C d\Omega_c} = KF \left| W(\vec{Q}_{Bs}) \right|^2 \frac{16\pi^2}{k_{ax} Q_{Aa}} \frac{v_{Cc}}{v_{ax}} \frac{d\sigma^{THM}}{d\Omega_{ax}} \tag{3.8}$$

with momenta

$$\hbar \vec{Q}_{Aa} = \vec{p}_{Aa} - \frac{m_A}{m_A + m_x} \vec{p}_{Bs} \tag{3.9}$$

$$\hbar \vec{Q}_{Bs} = \vec{p}_{Bs} - \frac{m_s}{m_b + m_x} \vec{p}_{Aa} \tag{3.10}$$

and the momentum distribution $W(\vec{Q}_{Bs})$ which is connected with the wave function of A in momentum space. In fact we can express it in terms of the momentum distribution of the "Trojan Horse particle" Φ_A by

$$W(\vec{Q}_{Bs}) = \left(E_A - \frac{\hbar^2 Q_{Bs}^2}{2\mu_{xs}} \right) \Phi_A(\vec{Q}_{Bs}) \tag{3.11}$$

[1] In the surface approximation the wave function $\Psi_{Cc}^{(-)}$ can be replaced by its asymptotic form.

with the binding energy $E_A < 0$. The momentum $\hbar\vec{Q}_{Bs}$ is directly related to the momenta of the spectator and transferred particle after the breakup. The cross section, written in terms of:

$$\frac{d\sigma^{THM}}{d\Omega_{Cc}}(Cc \to ax) = \frac{1}{k_{Cc}^2}\left|\sum_l (2l+1)P_l(\hat{Q}_{Aa}\cdot\hat{k}_{Cc})\left[S_l J_l^{(+)} - \delta_{(ax)(Cc)}J_l^{(-)}\right]\right|^2, \tag{3.12}$$

where δ is the Kronecker symbol, looks similar to a usual two-body cross section except for the functions $J_l^{(\pm)}$. They can be well approximated for our purpose by

$$J_l^{(\pm)} = D_l k_{ax} Q_{Aa} R^2 e^{\mp i\sigma_l}\left[G_l(k_{ax}R) \pm iF_l(k_{ax}R)\right] \tag{3.13}$$

where D_l is a constant, F_l and G_l are regular and irregular Coulomb functions, σ_l is the Coulomb phase shift in partial wave l and R is a cut-off radius originating from the surface approximation. The argument of the Legendre polynomial P_l is just the cosine of the center-of-mass scattering angle for the two-body reaction.

The analysis is simplified if the reaction of astrophysical interest is a non-elastic two-body process with different initial and final channels such that the $J_l^{(-)}$-term in eq 3.12 is zero. Assuming that only one partial wave l contributes dominantly to the cross section we find in this case [Spitaleri et al. (2001)]

$$\frac{d^3\sigma}{dE_C d\Omega_C d\Omega_c} = KF\left|W(\vec{Q}_{Bs})\right|^2 \frac{v_{Cc}}{v_{ax}} P_l^{-1} C_l \frac{d\sigma_l}{d\Omega_{ax}}(Cc \to ax) \tag{3.14}$$

with the usual on-shell two-body cross section $\frac{d\sigma_l}{d\Omega_{ax}}$ for the reaction $C + c \to a + x$ in partial wave l and a constant C_l. The essential feature is the appearance of the Coulomb penetrability factor

$$P_l(k_{ax}R) = \frac{1}{G_l^2(k_{ax}R) + F_l^2(k_{ax}R)} \tag{3.15}$$

which compensates for the strong suppression in the two-body cross section at small energies due to Coulomb repulsion. The obtained expression (3.14) is similar to the result in PWIA which was applied in earlier applications of the THM (see eq. 3.3) and corresponds to the heuristic approach in PWIA where one also corrects the extracted two-body cross section for the effect of Coulomb penetration (see previous section). Because of the factor C_l and the surface approximation, the two-body cross section can only be obtained with an arbitrary normalization but the essential energy dependence can thus be extracted. Absolute cross sections can be obtained by normalization to directly measured excitation function, at energies above the Coulomb barrier.

3.4 Experimental applications of the THM

The main aim of the THM is to extract a two-body cross section at low interaction energies from a three body one. In order to do this a kinematically complete experiment must be performed; this means that energies angular position of two of the outgoing particles and the energy of one of them, at least, must be known (as well as particle identification). As we will extensively explain in the next chapters, a THM experiment requires coincidence detection of particles c and C around suitable angles, the so-called "quasi-free pairs[2]"; moreover a suitable Trojan Horse particle, which has a high probability to be clustered into $A = x \oplus s$, is required. From experimental data (energy and angular position of both c and C), the relative energy E_{cC} can be calculated as well as the energy of the participant particle, E_x in the "post form" prescription:

$$E_x = E_{cC} - Q_{2b} \tag{3.16}$$

where Q_{2b} is Q-value for the two-body reaction.

Then applying equation 3.14 (or following equation 3.4 in the PWIA approach) it is possible to obtain, apart from a normalization constant, the two body $a + x \rightarrow c + C$ reaction cross section from the measured three body reaction one. The bare

[2] The angular conditions for c and C, where the quasi-free process is more probable, are referred to as quasi-free pairs.

nucleus cross section is extracted after a normalization to the two-body direct data at energies higher than the Coulomb barrier.

3.4.1 Validity test

As a first step data extracted via the THM must reproduce direct data at energies above the Coulomb barrier. In figure 3.4 it is shown, as an example, the comparison with direct data for the reaction $^7Li + p \rightarrow \alpha + \alpha$; within the experimental errors the comparison seems fair enough [Zadro et al. (1989)].

The same methodology was applied to the study of the quasi-free scattering $^6Li+^{12}C \rightarrow \alpha+^{12}C+d$ [Spitaleri et al. (2000)]; which allows to extract information on the cross section for the elastic scattering $\alpha +^{12} C \rightarrow \alpha +^{12} C$ (see figure 3.5).

In both cases we see a nice agreement between direct and THM data over all the explored energies. After this check it is possible to extend measurements at astrophysical energies.

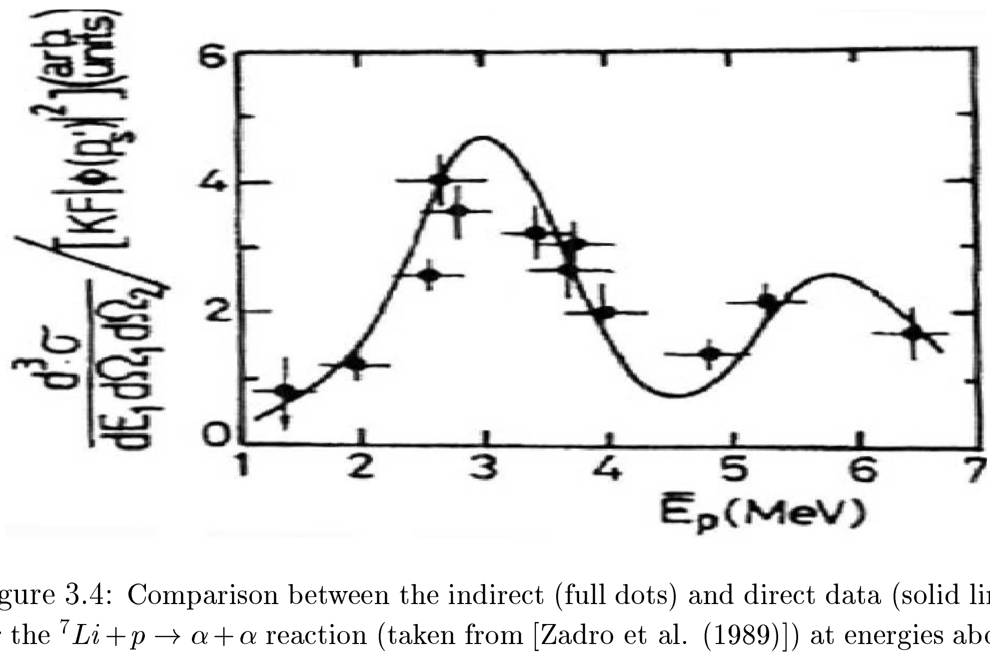

Figure 3.4: Comparison between the indirect (full dots) and direct data (solid line) for the $^7Li+p \rightarrow \alpha+\alpha$ reaction (taken from [Zadro et al. (1989)]) at energies above the Coulomb barrier.

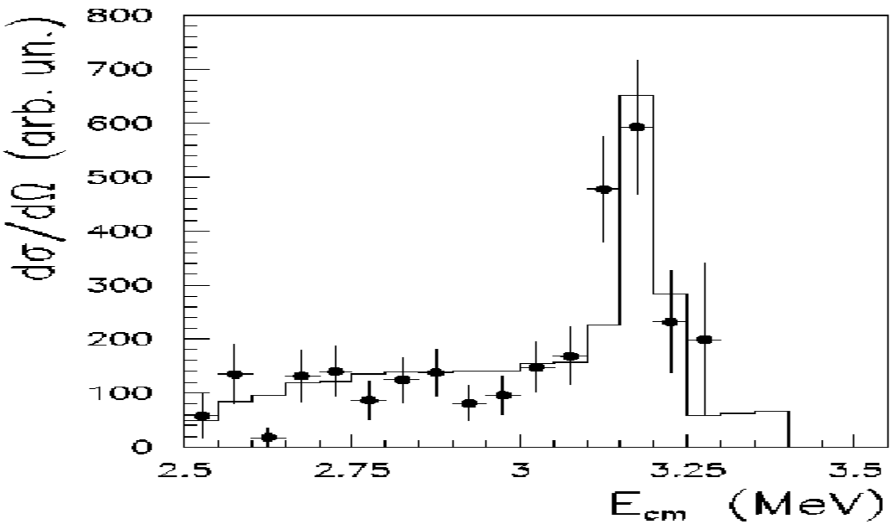

Figure 3.5: Comparison between the indirect (full dots) and direct data (solid line) for the scattering $^{12}C + \alpha \rightarrow \alpha +^{12} C$ (taken from [Spitaleri et al. (2000)]).

3.4.2 Applications

We remark the independence of the THM from direct data; however THM has to be seen as a complementary tool in experimental nuclear astrophysics because direct data are needed at energies above the Coulomb barrier for normalization procedure.

It has already been applied to the indirect study of various reactions at astrophysical energies. Here we report some examples:

- the $^6Li + d \rightarrow \alpha + \alpha$ (figure 3.6) reaction studied via the three-body reaction $^6Li +^6 Li \rightarrow \alpha + \alpha + \alpha$ [Cherubini et al. (1996)];

- $^7Li + p \rightarrow \alpha + \alpha$ (figure 3.7) reaction studied via the $^7Li + d \rightarrow \alpha + \alpha + n$ reaction [Calvi et al. (1997), Spitaleri et al. (1999)].

In pictures 3.6 and 3.7 it is possible to see a satisfying agreement between direct data [Engstler et al. (1992)] and the Trojan Horse one. In particular in pictures 3.6

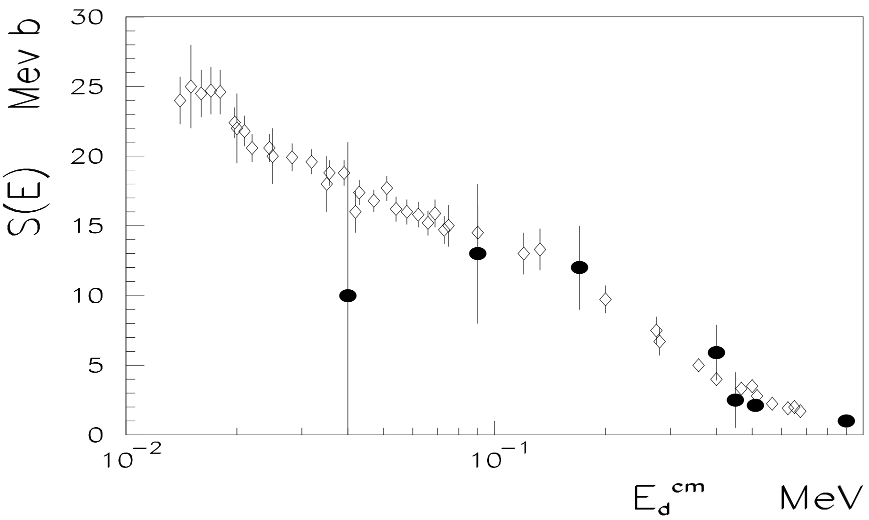

Figure 3.6: Comparison between the indirect [Cherubini et al. (1996)] and direct data [Engstler et al. (1992)] for $^6Li + d \rightarrow \alpha + \alpha$.

and 3.7 it has to be stressed how data suffer large error-bars; however the agreement between the three pair of data is nice within the experimental errors.

In order to improve these results and obtain more reliable astrophysical information, new measurements have been performed for $^6Li + d \rightarrow \alpha + \alpha$ reaction and other data have been analyzed for $^7Li + p \rightarrow \alpha + \alpha$ reaction. These results, which constitute the main experimental achievements of this thesis, will be discussed in the following chapters.

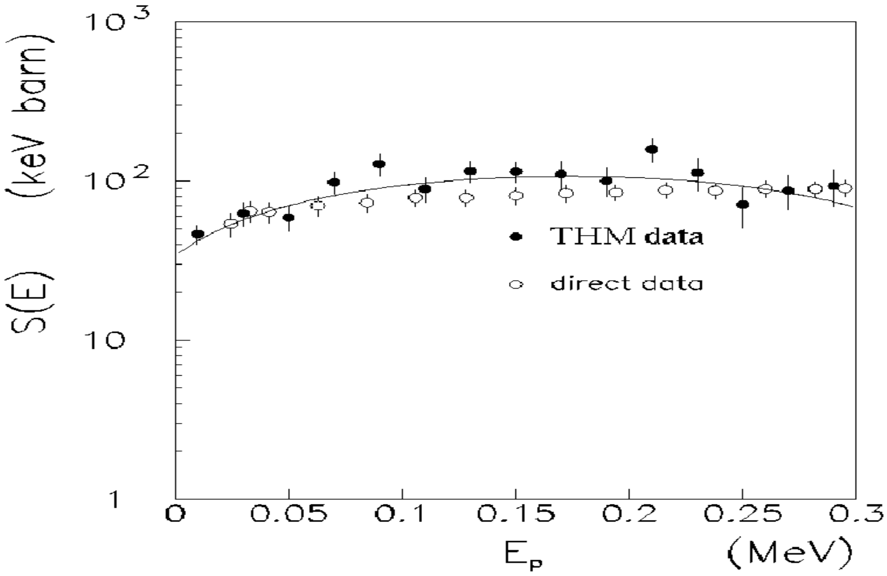

Figure 3.7: Comparison between the indirect [Spitaleri et al. (1999)] and direct data [Engstler et al. (1992)] for $^7Li + p \rightarrow \alpha + \alpha$.

Chapter 4

Indirect study of the $^6Li(d,\alpha)^4He$ reaction

One of the possible destruction mechanisms of ^6Li in the framework of the Inhomogeneous Big Bang Nucleosynthesis is the $^6Li(d,\alpha)^4He$ reaction [Applegate et al. (1988), Malaney & Fowler (1988)]; the energy corresponding to the Gamow peak, in these astrophysical conditions, is $E_{cm} \sim 300$ keV. A new experimental approach, based on the Trojan Horse Method will be presented in the following sections in order to measure the bare nucleus S(E)-factor and the electron screening potential for this process.

Data concerning the $^6Li(d,\alpha)^4He$ are extracted from a suitable three body reaction, $^6Li(^6Li,\alpha\alpha)^4He$; in particular it will be assumed that ^6Li, which has a high probability to be clustered in $^6Li = \alpha + d$ [Jain et al. (1970)], behaves like a Trojan Horse, either in the target or in the projectile. The beam energy, E_b=5.9 MeV, was chosen higher than the Coulomb barrier, in order to fulfill the THM hypotheses (see chapter 3).

4.1 Experimental setup

The experiment [Spitaleri et al. (2001)] was performed using the EN Tandem Van de Graaff accelerator at the Institut Rudjer Bošković in Zagreb. A $^6\mathrm{Li}^{2+}$ beam at 5.9 MeV was used to bombard an isotopically enriched $^6\mathrm{Li}_2\mathrm{O}$ target (125 μg/cm^2 thick), evaporated onto 20 μg/cm^2 carbon backing and oriented with its surface normal at 50° with respect to the beam axis. The beam current ranged between 10 and 15 particle nA and the beam spot on target after collimation had a diameter of about 2 mm. A silicon detector (monitor), placed at θ=40°, was used to detect the elastically scattered particles, thus allowing for a continuous monitoring of the target thickness during the experiment.

Since the Q-value for $^6\mathrm{Li}(^6\mathrm{Li},\alpha\alpha)^4\mathrm{He}$ (Q=20.896 MeV) is much larger of other possible three-body reactions occurring on lithium, carbon, oxygen or impurities in the target, the α-α coincident events are kinematically well separated and no particle identification was needed. The outgoing α particles were therefore detected using three 50×10 mm^2 silicon position sensitive detectors (PSD) centered at opposite sides of the beam axis at angles of 60° (PSD1), $-73°$ (PSD2) and $-103°$ (PSD3), as reported in table 4.1 (see also figure 4.1).

The choice of these angles was determined according to the three-body kinematics for the emission of the two α particles in the quasi-free assumption of a break-up process either in the target or in the projectile. In order to increase the solid angles with respect to the previous measurement [Cherubini et al. (1996)], the detectors were placed closer to the target and covered solid angles $\Delta\Omega_1 = 13.3$ msr (PSD1) and $\Delta\Omega_2 = \Delta\Omega_3 = 13.3$ msr (PSD2 and PSD3).

The angular range covered by each detector ($\Delta\theta \sim 14°$) correspond to momentum values of the undetected "spectator" α particle ranging from ~ -100 MeV/c to ~ 100 MeV/c for both QF processes. This ensures that the bulks of the two quasi-free contributions fall inside the investigated regions. Detector signals were processed by standard electronic chains and sent to the acquisition system which

Detector	Angle (deg)	Angular range (deg)	Distance (cm)	Solid angle (msr)
PSD1	60	53÷67	19.4	13.3
PSD2	73	66÷80	19.5	13.3
PSD3	103	96÷110	19.5	13.3
Monitor	40	39.5÷40.5	18.3	~1

Table 4.1: Angular position, distances and solid angles for the three PSD's and the silicon detector used in the experiment.

allowed for the on-line monitoring of the experiment and the data storage on magnetic tape for off-line analysis. Coincidences of detector PSD1 with either PSD2 and PSD3 were taken as well as single events of the monitor detector.

4.2 Calibration of PSD's

A position sensitive detector, PSD, supplies information both on the position and the energy of the detected particle. The detectors, whose thickness was 500 μm, were chosen in order to stop completely the detected alpha particles within their sensible volume. The relative error in energy signal was 0.8% while in the position was 1%.

In order to calibrate the detectors both in position and energy, data were taken using an Americium α-source (E_α=5.486 MeV), elastic scattering on Au and C at energy E_b=5.9 MeV, as well as the reaction $^{2}H(^{6}Li,\alpha)^{4}He$. A typical position versus energy matrix is plotted in picture 4.2 for PSD1.

4.2.1 Angular calibration

For the angular calibration a grid was used with 18 equally spatiated slits; the matrix obtained after such a calibration run is reported in fig. 4.2. Central angular

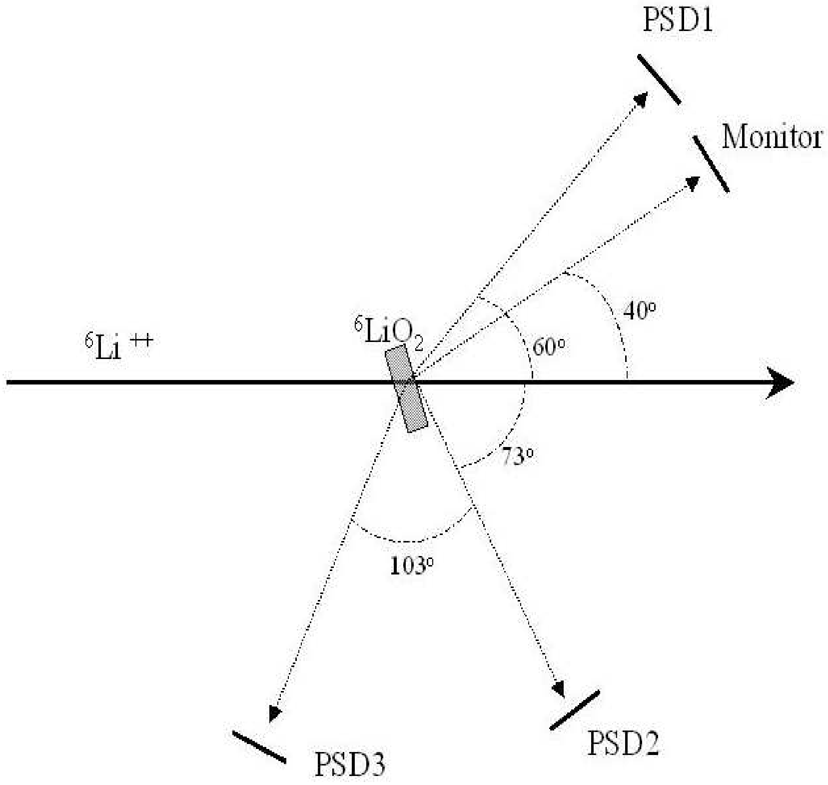

Figure 4.1: Experimental setup of the $^6Li(^6Li,\alpha\alpha)^4He$ experiment discussed in the text.

position of each detector θ_0 was measured using a theodolites; The angular position corresponding to each slit can be calculated by means of trigonometrical identities once the slits' spacing and distances from the detectors to the target are known.

For PSD the following relation has been applied to relate the position and energy signals:

$$x = \frac{P - P_0}{E - E_0}$$

where x is the energy-independent linear position and P_0 and E_0 are constant off-set to be determined using a fit.

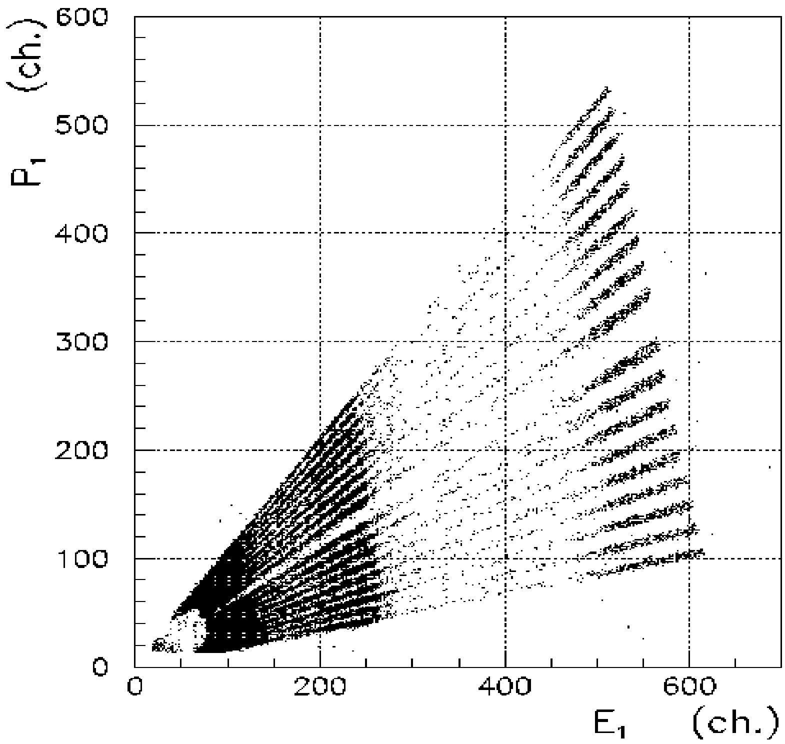

Figure 4.2: Position-energy matrix for detector one (calibration run); the 18 slits are clearly visible.

The angular calibration was performed using the correspondence between the position x_i of the i-th slit and the corresponding angle θ_i. The relation

$$\theta_i = \theta_0 + arctg[c_1(x_i - x_0) + c_2(x_i - x_0)^2]$$

was used with c_1, c_2, x_0 constants that must be calculated by means of a best fit.

4.2.2 Energy calibration

As a first approximation a simple linear relation between the PSD signal and the detected particle energy was used for the energy calibration. Further corrections were added to take into account the dependence of the energy signal from angular position. In order to establish the calibration parameters a fit was performed using, as calibration peaks, those belonging to the reactions cited above.

Energy loss in the target was also taken into account; in particular it was assumed that reactions take place at half target. The effective path was considered, taking into account the target beam-axis angle and the alpha's emission angles.

In picture 4.3 the calibrated angle-energy matrix is plotted for PSD1 for the same run as in fig. 4.2.

4.3 Data analysis

The first step one has to perform in the data analysis is the identification of the ^{6}Li(^{6}Li,$\alpha\alpha$)^{4}He and the separation of its contribution from that of other reactions that may take place within the same target. Due to the high Q-value (Q=20.896 MeV), the E_2 versus E_1 plot for the PSD1-PSD2 coincidence shows a kinematic locus which appears well separated from those corresponding to other possible contributing reactions (see fig. 4.4). This kinematic locus was then selected by means of a graphical cut and the corresponding events used for further analysis. The same was also done for the coincidence between detectors PSD1 and PSD3.

Moreover the Q-value spectra have been calculated event by event in order to check the calibration procedure and to help to discriminate the ^{6}Li(^{6}Li,$\alpha\alpha$)^{4}He from other reactions. A typical spectrum is shown in picture 4.5 and the events which have been analyzed were those corresponding to the peak at Q=20.896 MeV.

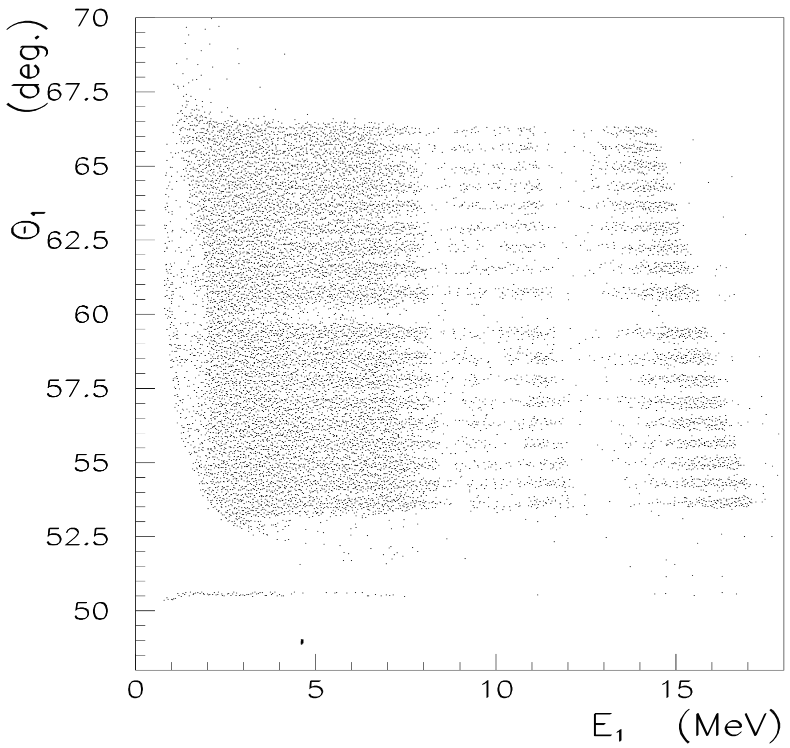

Figure 4.3: Calibrated position-energy matrix for PSD1 for a calibration run.

4.3.1 Angular correlations and relative energy spectra

All the coincidences between the detectors PSD1-PSD2 and PSD1-PSD3 were analyzed In order to check the presence of the quasi-free contribution angular correlations were produced. Angular correlation spectra were obtained by fixing one angle at a fixed value and considering different angles for the other detectors.

Figure 4.6 shows the angular correlation for coincidences between PSD1-PSD2 detectors is reported: in this case the angle of the first particle is fixed (θ_1=$60^o$$\pm$$0.5^o$) and $70^o \leq \theta_2 \leq 77^o$. As it was expected for a quasi-free mechanism [Spitaleri et al. (2001)]:

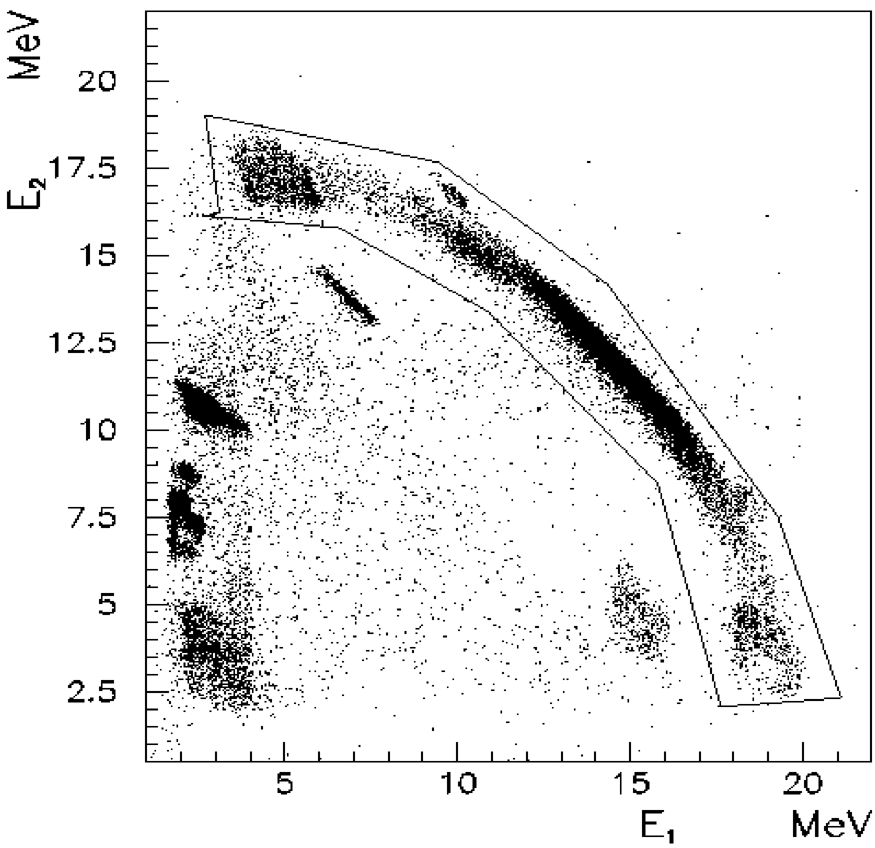

Figure 4.4: The kinematical locus of the ^{6}Li(^{6}Li,$\alpha\alpha$)^{4}He reaction for PSD1-PSD2 coincidences. The graphical cut is also shown.

- at the quasi-free pair, θ_1=60^o θ_2=73^o an enhancement is seen in correspondence of the condition[1] p_s=0 MeV/c;
- the peak vanishes as one moves far from the quasi-free pair. The same behaviour was observed for all the angular correlation spectra.

Spectra in relative energy E_{12} have also been plotted and in order to discriminate

[1] The impulse distribution of the spectator in ^{6}Li is peaked around p_s=0 MeV/c [Lattuada et al. (1988)]; this corresponds to the quasi-free condition for lithium target break-up.

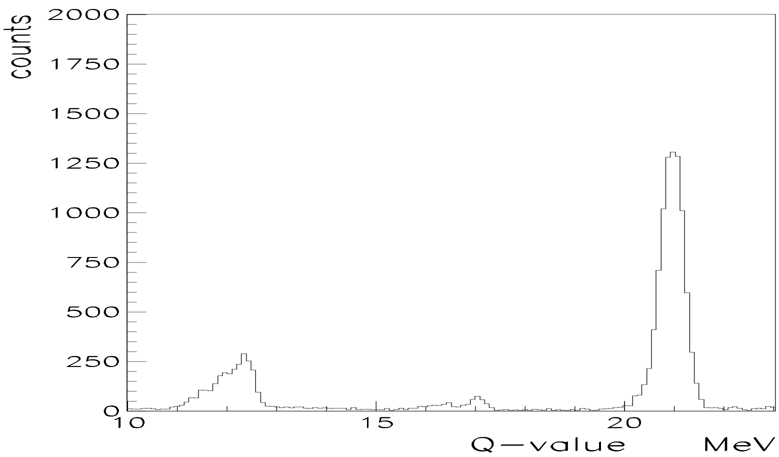

Figure 4.5: A typical Q-value spectrum. The large peak (at 20.896 MeV) corresponds to the ^{6}Li(^{6}Li,$\alpha\alpha$)^{4}He reaction.

possible contributions from sequential decays, cuts on p_s were taken, around the position p_s=0 MeV/c. As it is shown in figure 4.7 a large peak is present in correspondence of the quasi-free conditions, $|p_s| \leq 35$ MeV/c. As we move to different kinematic conditions (e.g. $|p_s| \geq 50$ MeV/c, see fig. 4.8) the peak decreases its intensity showing that sequential contributions can explain only a small fraction of the detected events.

From this evidence, from the width of the extracted momentum distribution and from the dependence of relative energy on p_s, we can conclude that at the specified angular pairs the quasi-free contribution is the dominant one.

4.3.2 Excitation function of the $^6Li(d,\alpha)^4He$ reaction

In figure 4.9 the three-body differential cross section, for target break-up, is plotted (full dots) in arbitrary units as a function of the interaction d-^6Li energy, defined

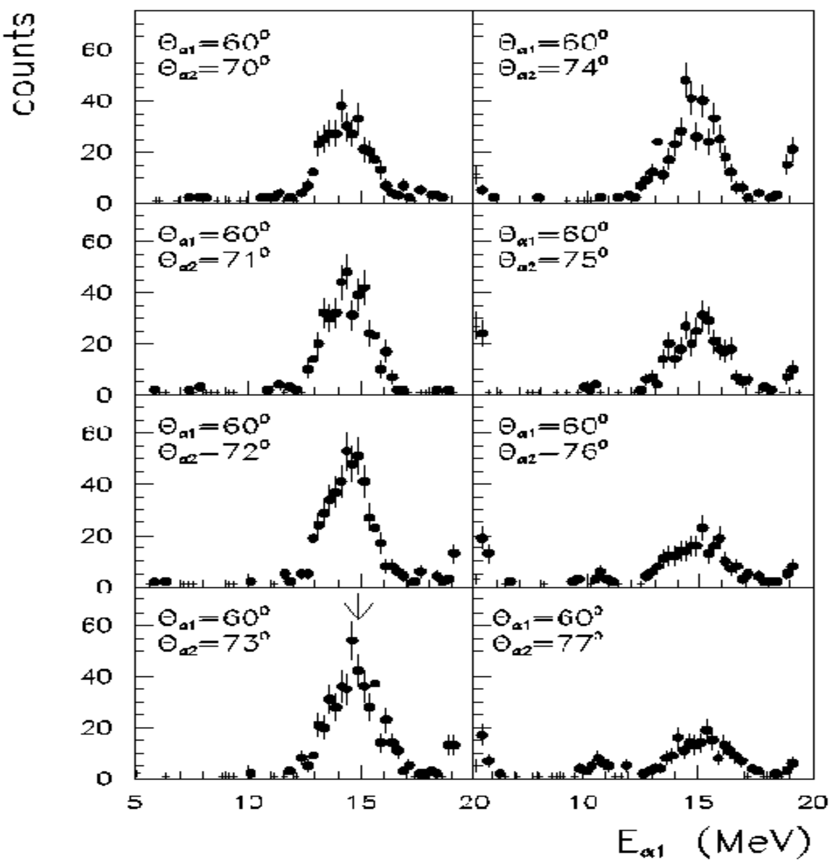

Figure 4.6: Angular correlation spectra for θ_1=60^o$\pm$0.5^o, and 70^o $\leq \theta_1 \leq$ 77^o. The arrow marks the energy corresponding to zero spectator momentum.

by eq. 3.16:

$$E_{d-{}^6Li} = E_{12} - Q_{2b}$$

with E_{12} the relative energy of the two detected alpha's and Q_{2b} the Q-value for the two body reaction (for the $^6Li(d,\alpha)^4He$ reaction $Q = 22.372$ MeV). It was obtained by selecting the events within the specified kinematic locus and the condition $p_s \leq$ 35 MeV/c. A comparison is made with data extracted from projectile break-up, whose data are shown as empty dots.

The two data-sets seem to be in agreement (except for a normalization constant)

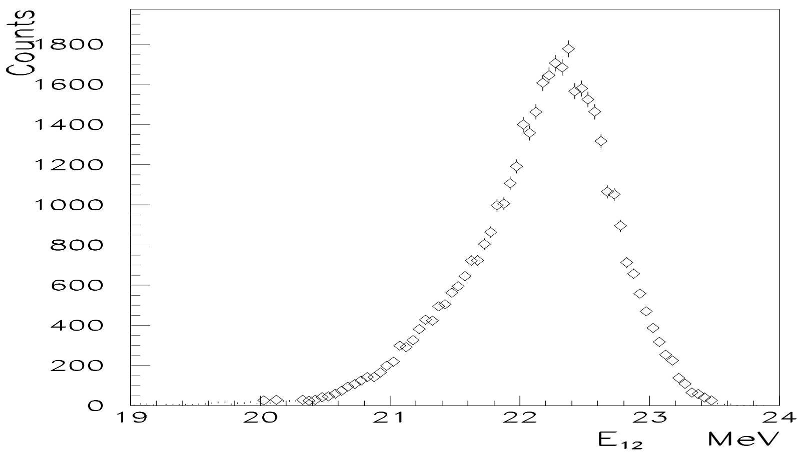

Figure 4.7: Relative energy E_{12} spectrum for events with $|p_s| \leq 35$ MeV/c.

as it was expected. This cross-check confirms the analysis which has been performed for both cases; moreover the two different data-sets carry two independent estimates which will be averaged, thus improving the significativity of the mean S-factor extracted.

4.4 Extraction of the astrophysical S(E)-factor

The astrophysical S(E)-factor, which has been defined according to equation 2.5, has been extracted for the $^6Li + d \to \alpha + \alpha$ reaction, both for the target and projectile break-up case.

Using the definition of the astrophysical factor (formula 2.5) in equation 3.14 and assuming a dominant s-wave contribution [Cherubini et al. (1996)] one obtains:

$$\frac{d^3\sigma}{dE_{\alpha_1} d\Omega_{\alpha_1} d\Omega_{\alpha_2}} = KF \left| W(\vec{Q}_{(\alpha_1\alpha_2)d}) \right|^2 \frac{C_0}{4\pi} \frac{\mu_{(Li-d)} k_{Li-d}}{\mu_{\alpha_1\alpha_2} k_{\alpha_1\alpha_2}} \frac{\exp\left(-2\pi\eta_{Li-d}\right)}{E_{Li-d} P_0(k_{Li-d}, R)} S(E_{Li-d}) \tag{4.1}$$

with notation introduced in chapter 3.

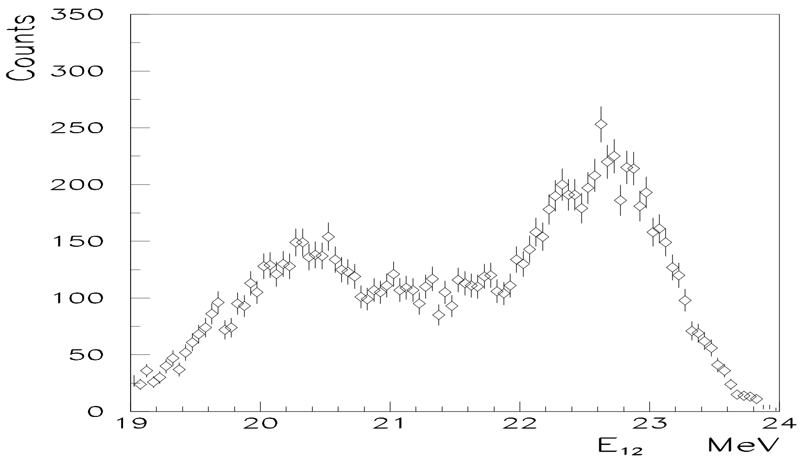

Figure 4.8: Relative energy E_{12} spectrum for events with $|p_s| \geq 50$ MeV/c.

A Monte Carlo simulation of the experiment was performed in order to calculate $\frac{d^3\sigma}{dE_{\alpha_1} d\Omega_{\alpha_1} d\Omega_{\alpha_2}}$ from 4.1; a constant S(E)-factor was assumed and all cuts in energy and scattering angle for the detected α particles, as given by the detector setup, were taken into account. Additionally, only events with spectator momenta $|p_\alpha| < 35$ MeV/c were selected. The inter-cluster momentum distribution of the ^6Li (the "Trojan Horse" particle), which is needed in order to calculate $\left|W(\vec{Q}_{(\alpha_1\alpha_2)d})\right|^2$ (see equation 3.11) is given by [Spitaleri et al. (2000), Spitaleri et al. (2001)] and references therein:

$$|\Phi_{Li}(q)|^2 = \frac{e^{-x}}{1+x} \qquad \text{with} \qquad x = \frac{q^2}{3555 \text{ fm}^{-2}}$$

with q the relative momentum of the α and d clusters inside ^6Li.

We also assumed a cutoff radius $R = 4.3$ fm which is calculated from the parameterization

$$R = r_0 \left(A_{Li}^{\frac{1}{3}} + A_d^{\frac{1}{3}} \right) . \tag{4.2}$$

with $r_0 = 1.4$ fm.

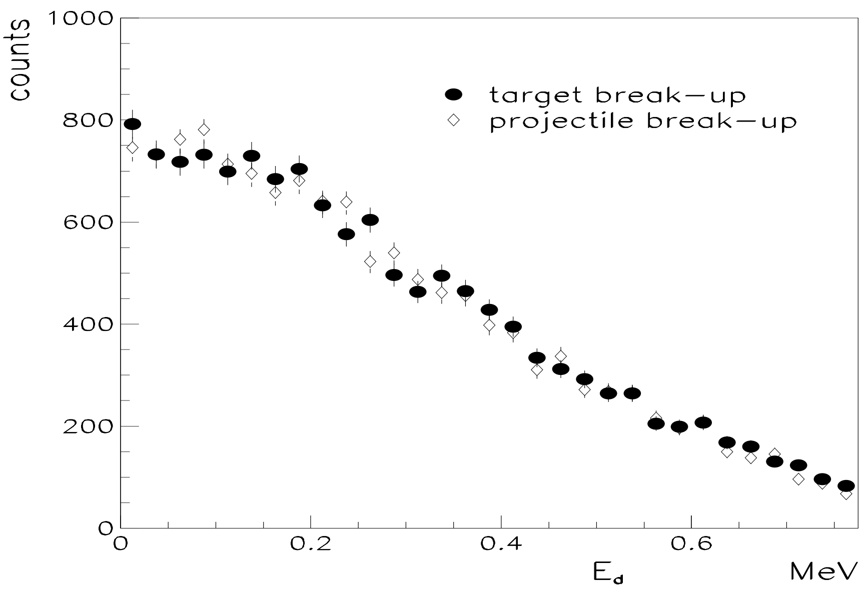

Figure 4.9: Three-body differential cross section plotted as a function of the d-^6Li interaction energy for the condition $|p_s| \leq 35$ MeV/c (full dots) for data extracted from target break-up. The open dots represent data extracted from the projectile break-up.

In order to get the energy dependence of the astrophysical S(E)-factor, the experimental three-body differential cross section (see figure 4.9), extracted for both sets of data (target and projectile break-up), was divided by the simulated one, inverting formula 4.1.

Statistical errors of the Monte Carlo Simulation were considered included in the errors relative to the S(E)-factors. These were normalized (e.g. fig. 4.10) to the direct data [Engstler et al. (1992)] in the energy range $600-700$ keV, where the electron screening effects are negligible and the two data sets are expected to overlap. In figure 4.10 the S(E)-factor of the ^{6}Li(d,α)^{4}He reaction obtained in the THM (target break-up) is compared with data from direct measurements [Engstler et al. (1992)].

In figure 4.11 the S(E)-factor of the ^{2}H(^{6}Li,α)^{4}He reaction obtained through the THM, from target and projectile break-up data, are compared after separate normalization.

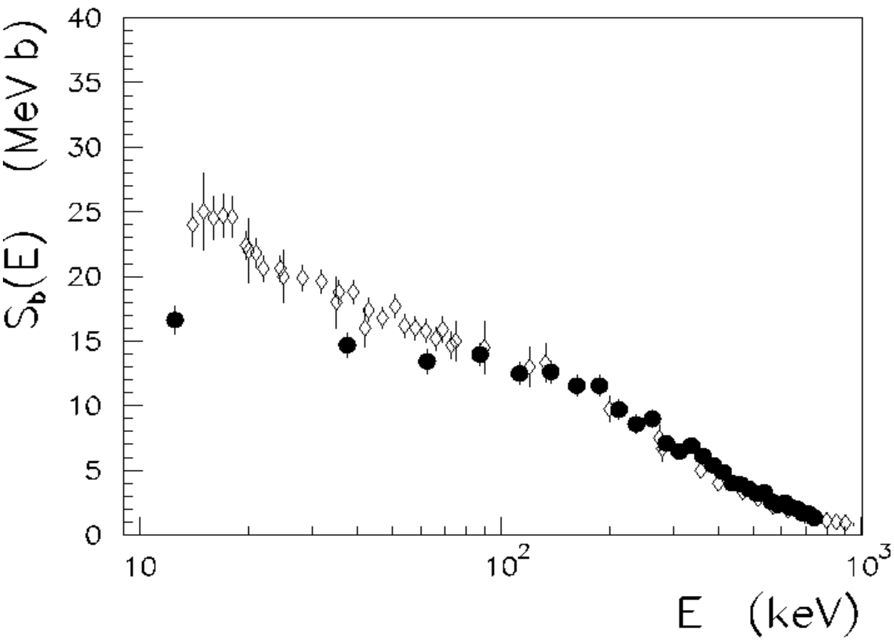

Figure 4.10: Astrophysical S(E) factor for the $^6Li(d,\alpha)^4He$ reaction. Data extracted, via THM, from target break-up (full dots) are compared to the direct data [Engstler et al. (1992)] represented by open symbols; the two data-sets are normalized between E= 600÷700 keV.

The total mean, weighted over respective errors, was calculated for data extracted from target and projectile break-up; thus the experimental errors were reduced due to an improved statistics. These results are plotted and normalized in figure 4.12 to direct data [Engstler et al. (1992)]. Following the discussion in chapter 3 it is possible to explain the discrepancy between the two data sets at energies E_d ≤100 keV by taking into account the electron screening effect in direct data (chapter 2). As already stressed, the THM gives directly the bare nucleus S-factor

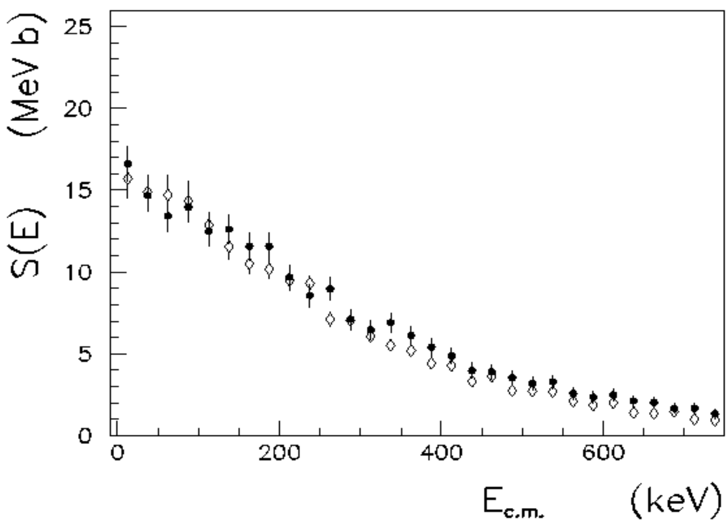

Figure 4.11: Astrophysical S(E) factor for the $^6Li(d,\alpha)^4He$ reaction. Data extracted, via THM, from target break-up (full dots) and projectile break-up (open symbols) are compared.

and no correction for the electron screening is needed in the data.

A polynomial fit of the averaged data was performed using a second order polynomial expression

$$S(E) = S(0) + S_1 \cdot E + S_2 \cdot E^2$$

this is plotted as a dashed line in picture 4.12. The mean parameters, together with the ones corresponding to fits to target and projectile break-up data are reported in table 4.2.

Different values of the cut-off radius R (different from R=4.3 fm) were also used to extract the astrophysical factor; in table 4.3 we report the fitting parameters for three different choices. As stated in [Spitaleri et al. (2001)] the extrapolated S-factor at zero energy, $S(0)$, remains in the range from 15.2 to 16.9 MeV·b, while changing

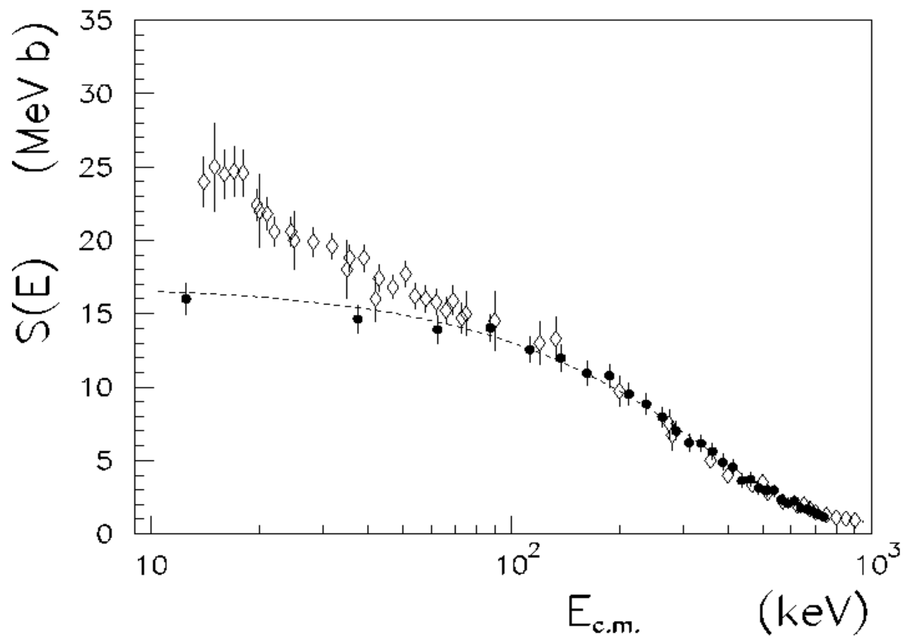

Figure 4.12: Astrophysical S(E) factor for the $^6Li(d,\alpha)^4He$ reaction obtained from the weighted mean of data extracted from target and projectile break-up (full dots). The dashed line represents a second order polynomial fit. The direct data (empty dots) taken from [Engstler et al. (1992)] are also shown for comparison.

R from 3.7 to 4.3 fm. This shows the sensitivity of the indirect method to changes in the parameter R; since the cut-off corresponds to the interaction radius in the $^6Li + d$ system the largest value R=4.3 fm was chosen according to [Evans (1969)].

Coefficients	target break-up	proj. break-up	mean
$S(0)$ (MeV·b)	16.9±0.5	16.7±0.5	16.9±0.5
S_1 (b)	-39.9	-43.0	-41.6
S_2 (MeV^{-1}·b)	26.1	30.2	28.2

Table 4.2: Fitting parameters for the S(E)-factors extracted from target and projectile break-up; the parameters of the fit to the weighed mean are also reported in the third column.

Coefficients	R = 3.7 fm	R = 4.0 fm	R = 4.3 fm
$S(0)$ (MeV·b)	15.2±0.5	16.1±0.5	16.9±0.5
S_1 (b)	-33.2	-36.9	-39.9
S_2 (MeV^{-1}·b)	19.9	23.6	26.1

Table 4.3: Coefficients of a second order polynomial fit on the S(E)-factors extracted from the target break-up [Spitaleri et al. (2001)], according to the different values of cut-off radius used for the calculation.

Chapter 5

The $^7Li(p,\alpha)^4He$ reaction studied via the THM

The same analysis performed on the $^6Li + d \to \alpha + \alpha$ experiment, was used for the $^7Li + p \to \alpha + \alpha$, a crucial reaction in astrophysics (see chapter one). In order to measure the bare astrophysical factor as well as the electron screening potential for the $^7Li + p \to \alpha + \alpha$, the three-body reaction, $^7Li + d \to \alpha + \alpha + n$ (d is the "Trojan Horse particle") has been chosen.

The Gamow peak for the $^7Li + p \to \alpha + \alpha$ reaction corresponds to a range $E_{cm} = 4 \div 250$ keV; thus it is necessary to correctly evaluate the electron screening effect in this energy range.

5.1 Experimental set-up

The ^7Li+$d \to \alpha$+α+n reaction was studied in a first experiment [Calvi et al. (1997)] at $E_{^7Li} = 20$ MeV, using ionization chambers as transparent Δ-E detectors in front of the PSD's at $\theta_{lab} = +45°(\pm\ 2°)$ and - $45°(\pm\ 2°)$ with respect to beam axis. However, due to the high Q value of the ^{7}Li(p,α)^4He reaction, the condition of α-α coincidences alone has shown to provide already a good separation of the events of interest, even without particle identification.

Thus, a second experiment that is described here, was performed using only PSD's, which allowed in turn for an improved energy resolution.

In figure 5.1 the experimental set-up is shown. The 15MV SMP Tandem Van de Graaff accelerator of the Laboratori Nazionali del Sud - Catania, provided a ^{7}Li-ion beam at energies 19, 19.5, 20, 21, 22, and 25 MeV and typical current 10 particle nA. The energy spread of the beam was about 10^{-4}% and the spot on target, after collimation, had a diameter of $\sim$ 1.5 mm.

During the experiment several deuterated polyethylene targets had to be used because of deuterium degradation problems; their thickness (average value $\sim$250 $\mu g/cm^2$) was determined using an Am source. Target thickness was constantly monitored using a silicon detector placed at a distance d=50.5 cm from the target and at $\theta = 18.5°$ with respect to the beam axis, in order to detect the elastically scattered particles. The reaction products were detected by using a set of 6 PSD's, centered at mean laboratory angles θ_{lab} = +44° (± 3°), +34° (± 5°), 23° (± 5°), -45° (± 3°), -55° (± 5°) and -65° (± 5°), where the number in brackets indicate the angular range covered (see table 5.1).

The central angles for the 6 PSD's were chosen by calculating the quasi-free pairs for the selected beam energies. The good angular resolution, typically 0.1° for each PSD, is needed for an improved analysis using the THM. Coincidence events were recorded between all pairs of detectors placed on opposite sides of the beam axis.

5.2 Calibration of the PSD's

The signals coming from the detectors were processed by using standard electronic chains and sent to the acquisition system which allowed the on-line monitoring of the experiment and the storage of data on magnetic tapes for later data off-line analysis.

At the initial stage of the measurement, position calibration runs where per-

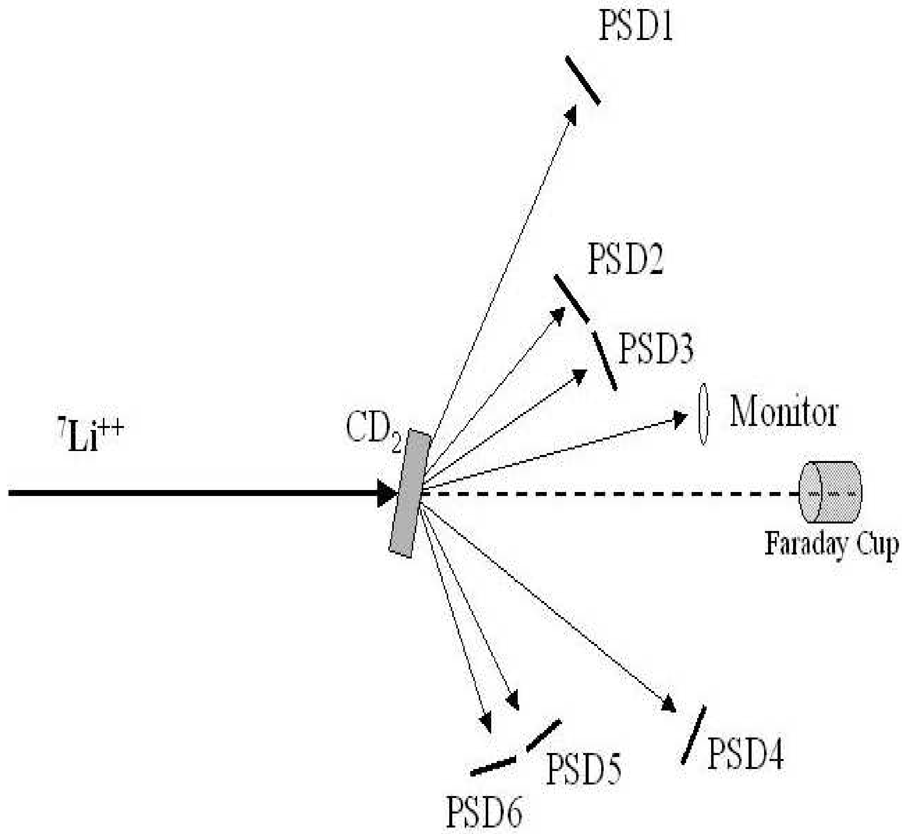

Figure 5.1: Experimental setup of the $^{7}Li(d,\alpha\alpha)n$ experiment discussed in the text. The positions of the detectors are reported in table 5.1.

formed placing grids, each one with 16 equally spaced slits in front of each PSD. In figure 5.2 a typical position versus energy matrix is reported for PSD1. A correspondence between position signals from the PSD's and angles of detected particles was therefore established as explained in chapter 4. Energy calibration was performed by means of a standard three-peak alpha source at energies of 5.155, 5.484 and 5.806 MeV. At higher energies the elastic scattering of ^{7}Li on carbon, deuterium and gold was employed at beam energies of 15, 20 and 25 MeV. We refer to the previous chapter for further details on angular and energy calibration, being the adopted

Beam energies (MeV)	Detectors	Angular ranges	Distance (cm)
19, 19.5, 20	PSD3 ÷ PSD6	$18^o \div 28^o$ $-60^o \div -70^o$	40
	PSD2 ÷ PSD5	$29^o \div 39^o$ $-50^o \div -60^o$	40
	PSD1 ÷ PSD4	$41^o \div 47^o$ $-42^o \div -48^o$	75

Table 5.1: Experimental conditions for the $^7Li + d \rightarrow \alpha + \alpha + n$ experiment discussed in the text.

procedure the same.

A typical calibrated position-energy matrix is shown in figure 5.3 for PSD1.

5.3 Data analysis

Coincidences between PSD1-PSD4 and PSD2-PSD5 have been analyzed for all the available beam energies during this thesis work, in order to extract the bare astrophysical S-factor and the electron screening potential.

Data analysis has been performed using the same procedure of that for $^6Li(d,\alpha)^4He$ reaction so we will frequently refer in the following to chapter 4.

Due to the high Q-value of the $^7Li(d,\alpha\alpha)n$ (Q=15.121 MeV) it has been possible also in this case to separate the contribution for this reaction from all the others occurring in the target. Via the same strategy reported in chapter 4 (see also [Spitaleri et al. (1999)] we have selected the kinematical locus of the $^7Li(d,\alpha\alpha)n$ 3-body reaction reported in figure 5.4.

A large peak is always present in correspondence of the 3-body Q-value of $^7Li(d,\alpha\alpha)n$ reaction. In figure 5.5 the Q-value spectrum for the coincidence between PSD1 and PSD4 at a beam energy of E_b=20 MeV is reported, and the peak at 15.121 MeV is clearly visible.

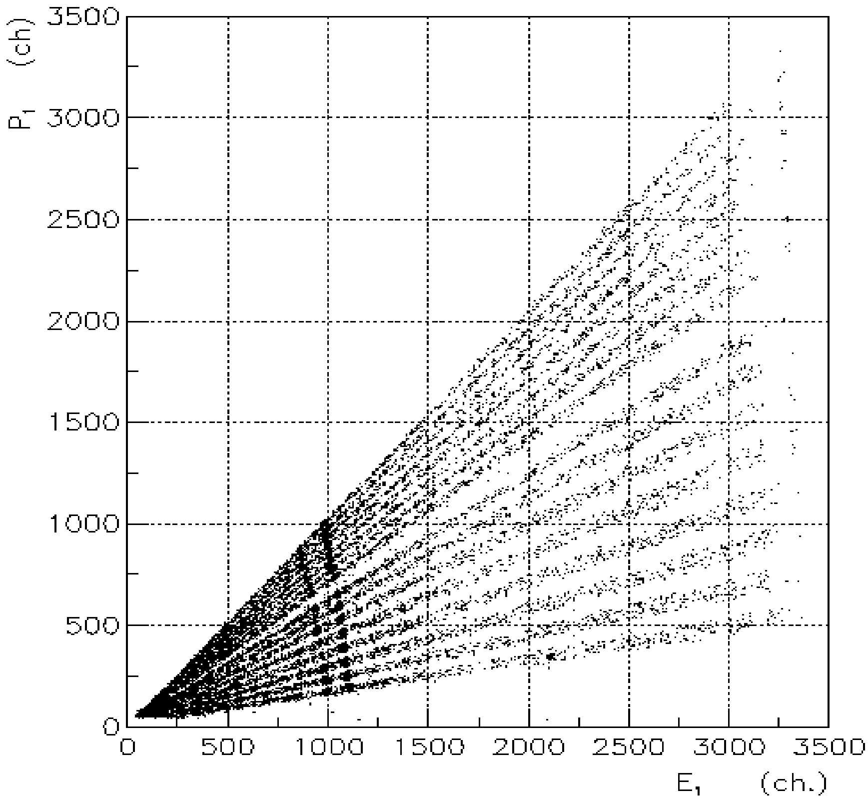

Figure 5.2: Position-energy matrix for PSD1 (calibration run, with grid).

5.3.1 Relative energy spectra

In order to distinguish the quasi-free contribution from sequential reaction mechanisms and to put in evidence possible contributions from formation of ^{8}Be and ^{5}He respectively, projections have been performed on the variables E_{12} (relative energy between the two outgoing α particles), E_{13} and E_{23} (relative energy between the neutron and each of the α particles). From such an analysis it has been found that the reaction ^{2}H(^{7}Li,$\alpha\alpha$)n mainly proceeds through formation of the 16.6 and 16.9 MeV levels of the ^{8}Be* as expected for the energy and angular conditions of the present measurement [Warner et al. (1987)].

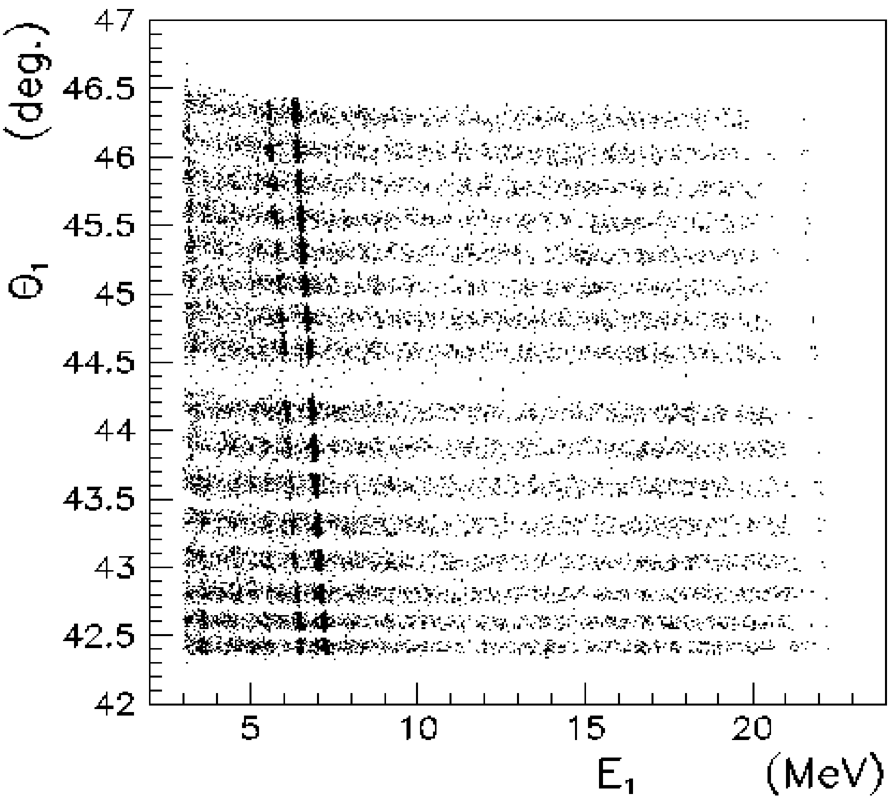

Figure 5.3: Calibrated position-energy matrix for PSD1 (calibration run, with grid).

The same procedure described above has been applied to PSD1-PSD4 and PSD2-PSD5 coincidences, for each beam energy: similar spectra have been obtained for events where a quasi-free contribution is expected. However, a small contribution, due to ^{5}He formation, has been observed in coincidences PSD3-PSD6 [Spitaleri et al. (1999)] and could overlap the energy region of the quasi-free mechanism. Therefore, in order to reduce the chance to have a systematic error related with the subtraction of such a contribution, only data analysis of coincidences between PSD1-PSD4 and PSD2-PSD5 has been worked out in this thesis.

In order to select the quasi-free contributions from other reaction processes a momentum p_s of the neutron spectator, $p_s \leq$40 MeV/c, has been chosen. Moreover

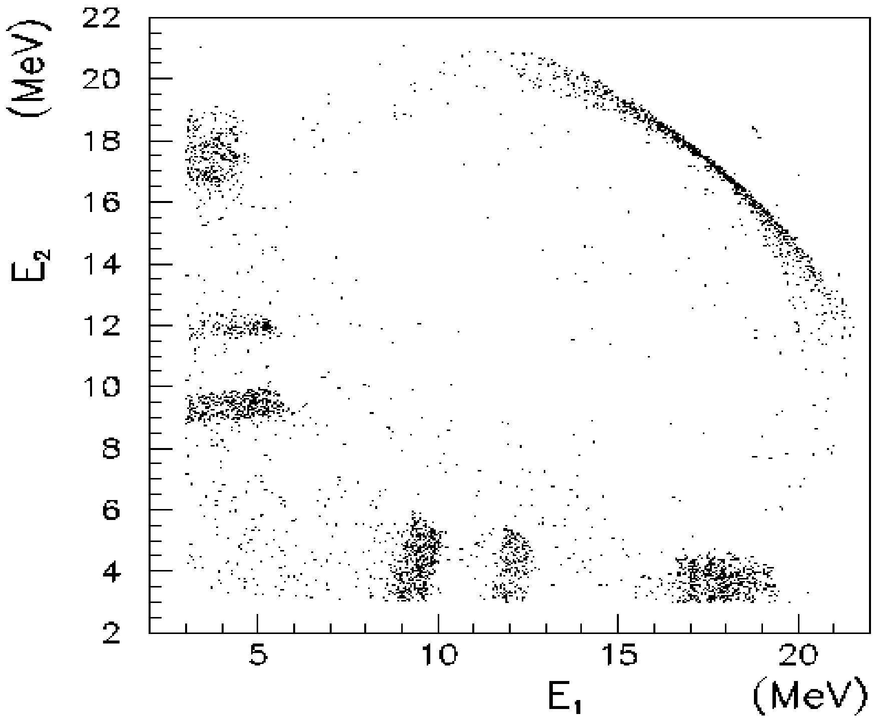

Figure 5.4: Kinematical locus for the $^7Li(d,\alpha\alpha)n$ in a E_2 vs. E_1 coincidence matrix between PSD1 and PSD4 (E_b=20 MeV).

only events whose $\alpha\alpha$ relative angle matches the quasi-free condition were considered (see table 5.2).

In fact, as we have seen in the previous chapter for the $^6Li(d,\alpha)^4$He reaction, the restriction to low p_s (e.g. $p_s \leq 40$ MeV/c) reduces the contribution of sequential processes to few percent of the total number of events [Lattuada et al. (2001)]. This is shown in figure 5.6.

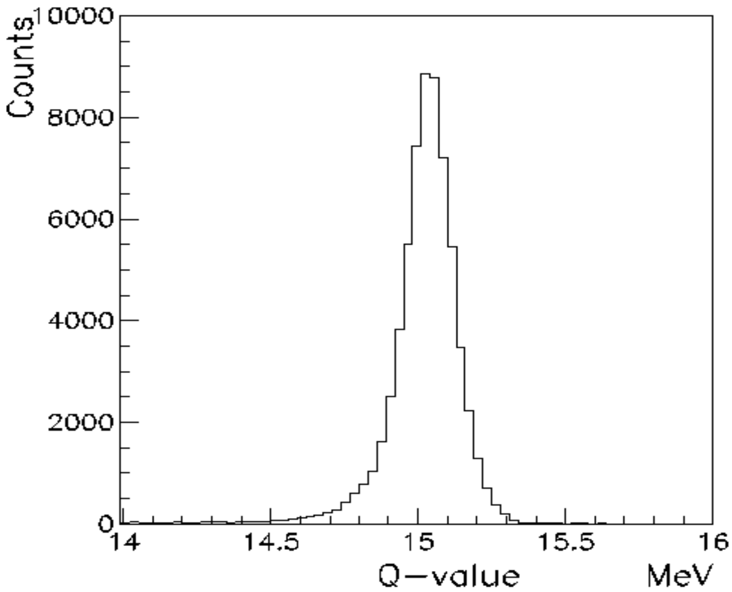

Figure 5.5: Q-value spectrum for the coincidence between PSD1 and PSD4 (E_b=20 MeV). The large peak is in correspondence of Q=15.121 MeV.

5.3.2 Three body cross section

In figures 5.7 the three-body cross section is plotted for E_b=20 MeV and for PSD1-PSD4 and PSD2-PSD5 coincidences. In such projection the variable

$$E_p = E_{12} - Q_{2b}$$

is adopted, as already defined in chapter 4 (here Q_{2b}=17.346 MeV, Q-value of the two body ^{7}Li(p,α)^{4}He reaction). The two sets of data (which are normalized to each other) agree fairly well, thus confirming the validity of the analysis performed. Results for other beam energies show the same trend and agree pretty well with the data at E_b=20 MeV.

These three-body excitation functions will be used for the extraction of the S(E)-factor, by using all the available data as it will be explained in the following section.

Beam energy (MeV)	Quasi free pairs ($\theta_1 + \theta_2$)
19	91.5
19.5	90.8
20	90.2

Table 5.2: Quasi free pairs, in terms of $\theta_1 + \theta_2$ for the different beam energies used in the experiment.

5.4 Extraction of the bare nucleus S(E)-factor

The bare nucleus astrophysical factor for the $^7Li(p,\alpha)^4$He has been extracted from the whole data set via the THM. The procedure is the same as that adopted for the $^6Li(d,\alpha)^4$He (chapter 4).

We have assumed a Hulthén wave function for the deuteron ground state

$$\Phi(\vec{r}_{p-n})_a = \sqrt{\frac{ab(a+b)}{2\pi(a-b)^2}}\frac{1}{r_{p-n}}\left(e^{-ar_{p-n}} - e^{-br_{p-n}}\right)$$

with parameters $a = 0.2317$ fm^{-1} and $b = 1.202$ fm^{-1} [Zadro et al. (1989)] and find the following result for the momentum wave function

$$\Phi(\vec{Q}_{(\alpha_1\alpha_2)n})_a = \frac{1}{\pi}\sqrt{\frac{ab(a+b)}{(a-b)^2}} \cdot \cdot \left[\frac{1}{a^2+Q^2_{(\alpha_1\alpha_2)n}} - \frac{1}{b^2+Q^2_{(\alpha_1\alpha_2)n}}\right] . \tag{5.1}$$

The parametrisation leads to a full width at half maximum of 57.4 MeV for $|\Phi_a|^2$. It has been already used in earlier applications of the THM [Spitaleri et al. (1999), Aliotta et al. (2000), Spitaleri et al. (2000)].

Thus using formula 4.1, through the same procedure already adopted for the $^6Li(d,\alpha)^4He$ and described in the previous chapter, we extract the bare astrophysical factor, S_b, for all the available energies and angular couples. We have assumed the cut-off radius R was calculated using the same parameterization and the same value for r_0 as reported in equation 4.2 for the ^6Li case.

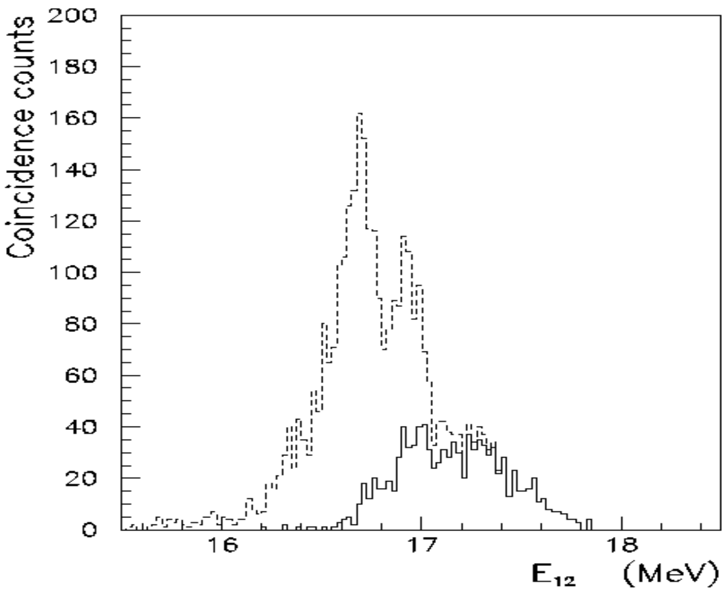

Figure 5.6: Coincidence events between the two α particles in the THM reaction ^{7}Li(d,$\alpha\alpha$)n at $E_{^7Li}$ = 20 MeV for detectors at $\theta_{lab} = 45^o \pm 0.75^o$ and $-45^o \pm 0.75^o$, as a function of relative energy E_{12} between the two α particles. The solid histogram shows the results restricted by the condition of a low spectator momentum ($p_s \leq 40$ MeV/c) and represents predominantly the case of the quasi-free process. Without this restriction, the energy region of the quasi-free process overlaps with the energy region of the sequential decay via the 16.6 and 16.9 MeV states in the compound nucleus ^{8}Be.

In figure 5.8 the normalized S_b is plotted for E_b=19, 19.5, 20 MeV. THM data were normalized to the direct ones [Engstler et al. (1992), Rolfs & Kavanagh (1986)] in the energy range $E_p = 300 \div 400$ keV.

The deduced S_b values, weighted average of all results, are plotted in figure 5.9 together with direct data from [Engstler et al. (1992)]. The normalization was carried out at energies E_p=300-400 keV. The THM has already been tested at energies above the Coulomb barrier as it is shown in figure 3.4

In figure 5.10 a theoretical curve from [Aliotta et al. (2000)] is shown; this was obtained from a fit with a superposition of direct and resonant contributions to the

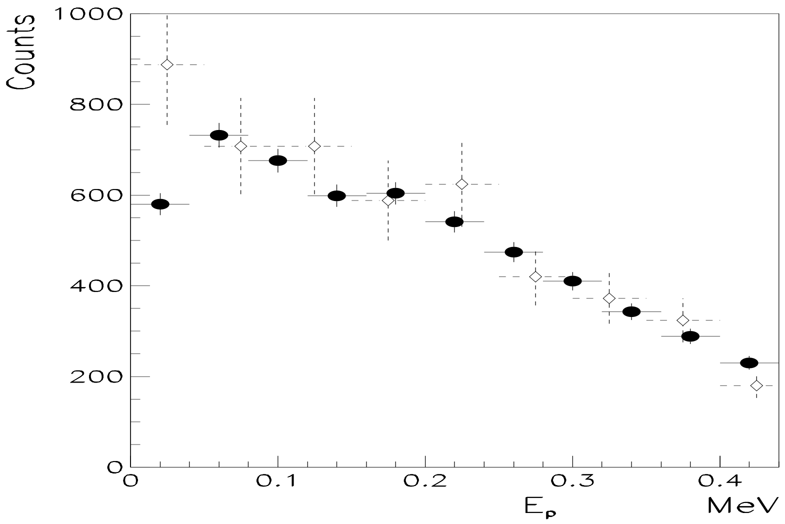

Figure 5.7: Differential three-body cross section extracted for E_b=20 MeV with $p_s \leq 40$ MeV/c. Data from PSD1-PSD4 (diamonds) and PSD2-PSD5 (circles) are compared.

direct experimental data for $E_p \geq 100$ keV.

Using the already known polynomial expression

$$S(E) = S(0) + S_1 \cdot E + S_2 \cdot E^2$$

to fit the S_b data as it is shown in picture 5.9 (dashed line), we obtain the parameters reported in table 5.3. In this table fitting parameters for the different beam energies are also reported together with a comparison with older data from [Calvi et al. (1997)]. The mean zero-order coefficient is S(0)= 55±3 keV b, where the quoted error represents the statistical one. The indirect data set also suffers from a systematic one, whose value is around 10%, arising from the normalization procedure.

THM data can be compared with previous estimates of the bare astrophysical factor from [Engstler et al. (1992)] which measured $S(0)_b \approx 58$ keV b, the same

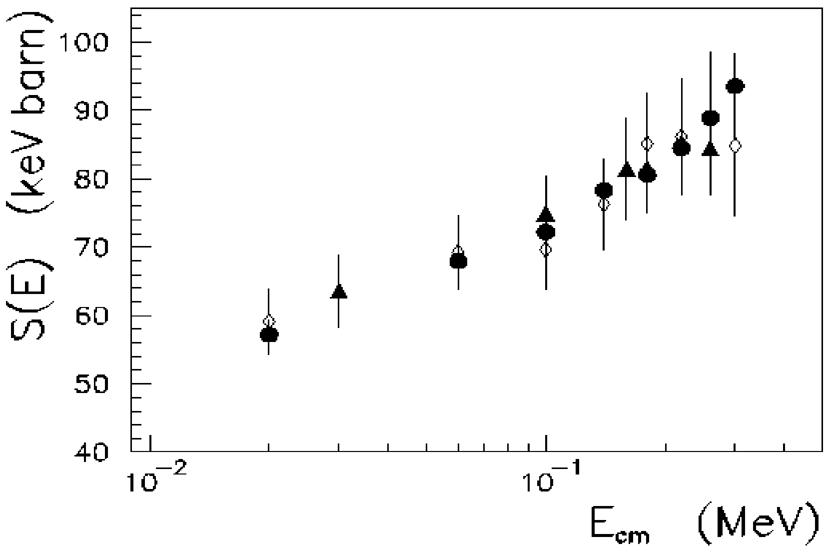

Figure 5.8: Bare astrophysical factor, S_b extracted from THM experiment at different beam energies: E_b=19 MeV (triangles), E_b=19.5 MeV (diamonds) and E_b=20 MeV (full circles).

value suggested by a recent R-matrix fit performed by F. Barker [Barker (2000)].

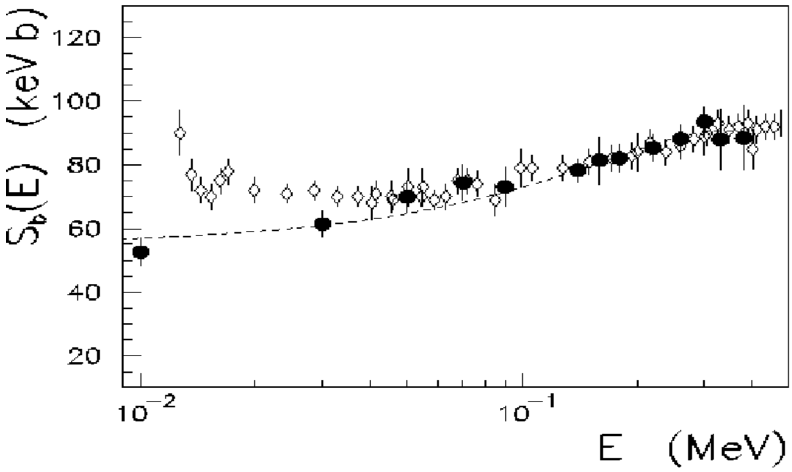

Figure 5.9: Bare astrophysical factor, averaged over the whole data-set compared to the direct measured one (diamonds) taken from [Engstler et al. (1992)]. The dashed line represents a second order polynomial fit.

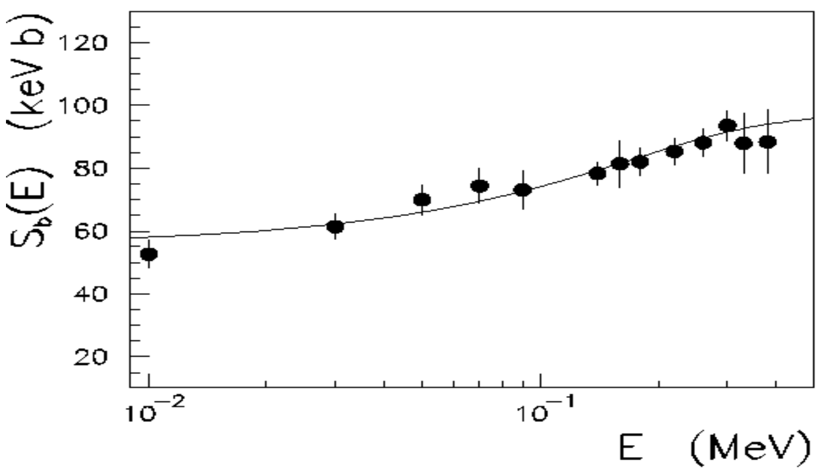

Figure 5.10: Bare astrophysical factor, averaged over the whole data-set. The solid line represents a theoretical calculation performed in [Aliotta et al. (2000)].

		[Calvi et al. (1997)][a]	Present work[b]			
E_{beam}	(MeV)	20	19	19.5	20	Mean
S(0)	[keV b]	53 $\pm$ 13	57 $\pm$ 8	55 $\pm$ 6	55 $\pm$ 3	55 $\pm$ 3
S_1	[b]	210	214	214	209	210
S_2	[keV^{-1} b]	-386	-422	-356	-304	-310

[a] Coincidences between one detector pair

[b] Weighted average of coincidences between nine detector pairs

Table 5.3: Fit parameters of the polynomial expression S(E)= S(0) + $S_1 \cdot$E + $S_2 \cdot$ E^2 applied to the THM data (E in units of MeV).

Chapter 6

Results

As already discussed in chapter 3 the THM offers the possibility to measure directly the bare nucleus astrophysical factor. By comparing the directly measured (screened) and the bare nucleus astrophysical factor (given by the THM) one may evaluate the screening potential U_e applying:

$$S_s = S_{THM} \cdot e^{\left(\frac{\pi \eta U_e}{E}\right)} \tag{6.1}$$

with S_s and S_{THM} the screened and bare S(E)-factor respectively and η the Sommerfeld parameter.

From this comparison a model-independent experimental estimate of the screening potential may be inferred.

6.1 Extraction of the electron screening potential for the $^6Li(d,\alpha)^4He$ reaction

This procedure has been applied to the averaged astrophysical S(E)-factor for the $^6Li(d,\alpha)^4He$ reaction. The best fit for the determination of U_e via equation 6.1 is shown in figure 6.1; direct data are taken from [Engstler et al. (1992)]. The fit gives an electron screening potential U_e=320±50 eV. This result can be compared to the one reported in [Engstler et al. (1992)], U_e=330 ± 120 eV (molecular target). We remark that we use a completely independent method to determine the screening potential and we observe the same systematic discrepancy observed in other cases [Engstler et al. (1992), Costantini et al. (2000)] with respect to the adiabatic approximation, which for the $^6Li + d \rightarrow \alpha + \alpha$ yields U_e^{ad}=186 eV.

In table 6.1 the values of the screening potential, separately extracted from projectile and target break-up are reported. Again we underline the agreement between the two data sets.

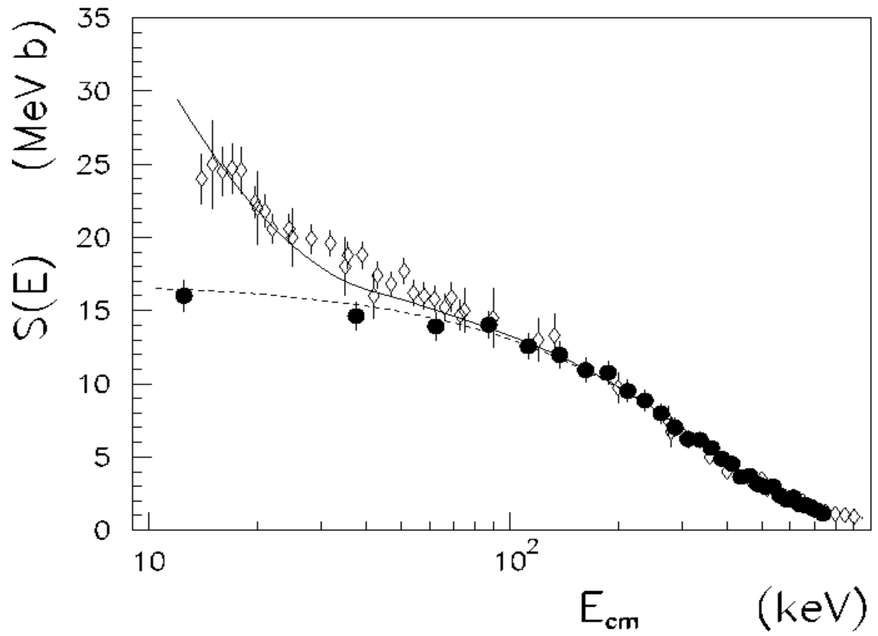

Figure 6.1: Astrophysical S(E) factor for the $^6Li(d,\alpha)^4He$ reaction averaged over data extracted via the THM from target and projectile break-up compared with direct data from [Engstler et al. (1992)]. The dashed line represents a second order polynomial fit to THM data while the solid line is the fit used for the determination of U_e.

	target break-up	proj. break-up	mean	adiabatic
U_e (eV)	340 ±51	336 ±58	320 ±50	186

Table 6.1: Evaluation of screening potential for the $^6Li(d,\alpha)^4He$ from the target and projectile break-up data sets. Results from the averaged data-set and the adiabatic value are also reported.

6.2 Determination of the electron screening potential for the $^7Li(p,\alpha)^4He$ reaction

As for the $^6Li(d,\alpha)^4He$ reaction, in the previous section, it will be assumed that the THM gives the bare nucleus astrophysical factor. According to formula 6.1, we find an independent estimate for the screening potential, by comparing our results with the direct ones [Engstler et al. (1992)]. The extracted value is U_e=330 ±40 eV and the fit to the shielded data is shown as a solid curve in figure 6.2.

This value must be compared with the screening potential extracted from direct measurements using the procedure described in chapter two (U_e= 300 ±160 eV [Engstler et al. (1992)], molecular target) and with the adiabatic value, U_e= 186 eV. As well as for the $^6Li(d,\alpha)^4He$ case a systematic discrepancy between experimental and theoretical value of the electron screening potential is confirmed; moreover the two independent determinations, the direct and indirect one, of the electron screening potential for the $^7Li(p,\alpha)^4He$ agree within experimental errors.

6.3 Conclusions

The results obtained both for the $^6Li(d,\alpha)^4He$ and the $^7Li(p,\alpha)^4He$ cases demonstrate how the THM can be applied in order to achieve independent and complementary information on the bare-nucleus cross section, as well as in the determination of the electron screening potential for these reactions.

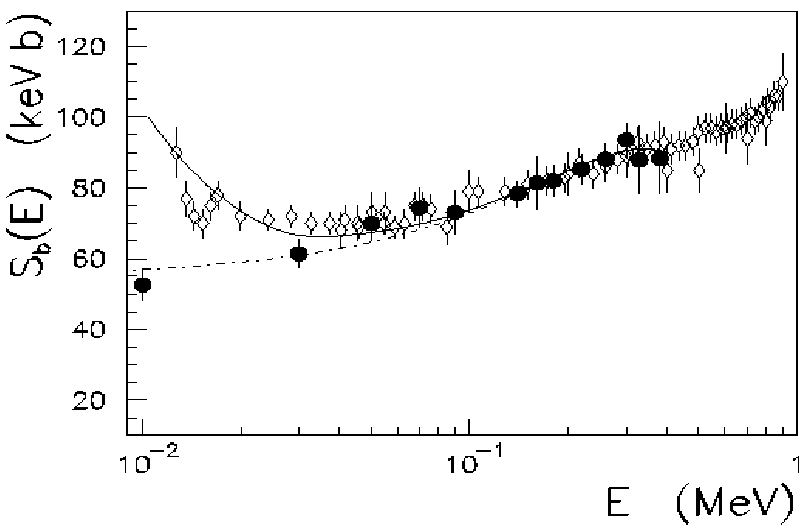

Figure 6.2: Bare astrophysical factor for the $^7Li(p,\alpha)^4He$ reaction, averaged over the whole data-set compared with direct data from [Engstler et al. (1992)]. The second order polynomial fit is plotted as a dashed line while the solid line represents the fitted screened contribution used for the extraction of U_e.

As regards the "Lithium problem" our results cannot solve the discrepancy between astrophysical models and observations. In particular the present results agree with previous direct measurements [Engstler et al. (1992)], already taken into account in the NACRE [Angulo et al. (1999)] compilation. This essentially leads to unchanged astrophysical conclusions (see next chapter).

As regards the electron screening effect, extrapolations at very low energy have been avoided by the use of the THM and previous values of U_e are confirmed with an improved precision. Moreover the systematic discrepancy between the theoretical and experimental values of U_e is still present, while no isotopical dependence [1] of the

[1] i.e. the electron screening effect is independent on the isotopes which are reacting.

	$^6Li(d,\alpha)^4He$	$^7Li(p,\alpha)^4He$	adiabatic
U_e (eV) THM	340 ±50	330 ±40	186
U_e (eV) direct	330 ±120	300 ±160	

Table 6.2: Results for the electron screening potential (in eV) for both the examined reactions measured via the THM and direct methods [Engstler et al. (1992)]. The adiabatic limit is also reported for comparison. The isotopic independence of U_e is clear within the experimental errors.

screening effect is found. These results are summarized in table 6.2 for the studied reactions.

The extracted value of U_e for the $^7Li(p,\alpha)^4He$ reaction is also significantly far from that required by [Castellani et al. (1996)] in order to explain the lithium depletion in the Hyades. A brief review of possible solutions to the lithium problem will be given in the following chapter.

In order to elucidate further possible systematic pitfalls in the THM, an experiment is in progress to study the ^{7}Li(p,α)^{4}He reaction via the THM reaction ^{7}Li(^{3}He,$\alpha\alpha$)^{2}H. Probing the same astrophysical reaction through a different three-body reaction can confirm the reliability of the method and offer a cross-check of the obtained results.

Similarly, the ^{3}He(d,p)^{4}He reaction (see chapter 2) will be investigated via the THM reaction ^{6}Li(^{3}He,$p\alpha$)^{4}He and an experimental investigation of the $^6Li(p,\alpha)^3He$ reaction is in progress in order to extract astrophysically relevant information by studying the ^{6}Li(d,α^3He)n reaction via the THM.

Chapter 7

Astrophysical Implications

The comparison of the present indirect measurement of the astrophysical S(E)-factor of the $^7Li + p \to \alpha + \alpha$ reaction with the most recent available data, e.g. [Engstler et al. (1992)] and the NACRE compilation [Angulo et al. (1999)], clearly shows that the two data sets are coherent. It was pointed out in [Swenson et al. (1994)] that only large changes on the $S_b(0)$ factor, with respect to the presently known value, could match the observation of lithium surface abundance for the Hyades, which is one of the best studied cases. Our result which confirms the previous extrapolations, is clearly from such a requirement.

Calculations were performed (see section 2 and [Castellani et al. (1996)]) in order to investigate the dependence of the calculated lithium abundance in the Hyades on the electron screening potential. A good agreement between theoretical models of lithium depletion and Hyades observations is obtained for U_e=600÷700 eV. Again both present measurements for $^7Li + p \to \alpha + \alpha$ and $^6Li + d \to \alpha + \alpha$ yield a lower value for U_e, coherently with [Engstler et al. (1992)].

Up to now we have pointed out that the THM and the direct measurement substantially give the same lithium abundance. Let us focus our attention on the solar lithium problem, which is, by far, the best studied case to investigate the sensitivity of the solar surface lithium abundance on the two different reaction rates.

7.1 The solar lithium problem

The present abundance on the solar surface is $\varepsilon = 1.16$ (which corresponds to a mass fraction of X(Li)=7.01×10^{-11}, [Anders & Grevesse (1989)], see the definition of abundances in chapter one). This value has to be compared with the meteoritic value, $\varepsilon = 3.31$ (corresponding to a mass fraction of X(Li)=9.88×10^{-9}, [Anders & Grevesse (1989)]). Since at the beginning of the solar system the protosolar nebula was homogeneous, the Sun has clearly depleted lithium of a factor 140. Many standard models [Swenson et al. (1994), Morel et al. (1997)] predict lithium abundances larger than the observed one. Again here we find a "lithium problem" i.e. the discordance between observed Li-abundance and the calculated one.

Solar models should reproduce the observed solar variables, such as luminosity and radius by adopting a set of physical and chemical inputs chosen within the range of their uncertainties. Helioseismology has allowed for a better understanding of solar interior and has added severe constraints to solar model calculations. More observables, e.g. the sound-speed or the depth of convective envelope, must be reproduced , thus improving the reliability of the model. For instance it has been shown that only a model which takes into account the microscopic diffusion[1] can explain the helioseismological observations [Castellani et al. (1997)].

The FRANEC code (Frascati RAphson Newton Evolutionary Code), which is extensively discussed in [Ciacio et al. (1997)], has been applied to calculate a solar model which includes the light elements' diffusion. In particular the lithium surface abundance at the present age ($t_\odot$=$4.6 \cdot 10^9$ years) was calculated taking into account both Pre-Main-Sequence and Main-Sequence lithium-depletion. This model was calculated using the OPAL equation of state [Rogers & Iglesias (1996)], using α =1.9, the mixing length parameter[2], the initial helium abundance Y=0.269 and

[1] Microscopic diffusion depends on different factors: gravity, temperature, concentration gradients.

[2] The parameter α takes into account the efficiency of the stellar convection and is defined

the metallicity Z=0.0198.

Since the evolution of lithium abundance will be described from the PMS phase, we took as initial value of lithium abundance the meteoritic value, $\varepsilon = 3.31$.

7.1.1 Li-depletion in the Sun during PMS

In section 1.4.1 it was pointed out that the PMS phase of stellar evolution can be a source of large lithium depletion especially for stars with $M \leq 1\ M_{\odot}$. Two different calculations have been performed using the FRANEC code: in the first case, it was adopted the cross section of the $^7Li(p,\alpha)^4He$ directly measured in [Engstler et al. (1992)] and used for the NACRE compilation. The second calculation was performed by changing the cross section to the one measured in this thesis, via the THM. As it was expected the difference is quite small and amounts to few percent. In figure 7.1 we report the trend of lithium abundance versus stellar age (expressed in units of 10^6 years) for the Sun during the PMS phase. The solid line represents the calculation performed using the rate of the $^7Li + p \rightarrow \alpha + \alpha$ extracted from the NACRE compilation while the dashed one represents that obtained adopting the cross section measured via the THM.

In both cases we can see how the main contribution to the lithium depletion for the Sun comes from the PMS lithium burning.

7.1.2 Li-depletion in the Sun during MS

The FRANEC code was used to calculate the lithium surface abundance during the main sequence. The same values of the PMS case were adopted for α, metallicity, primordial helium and the OPAL equation of state. Again we have performed two calculations, the first using the direct determination of the $^7Li(p,\alpha)^4He$ S(0)-factor, the second one using the THM determination extracted in the present work.

as $\alpha = l/H_p$ with l the mixing length and H_p the pressure scale-height.

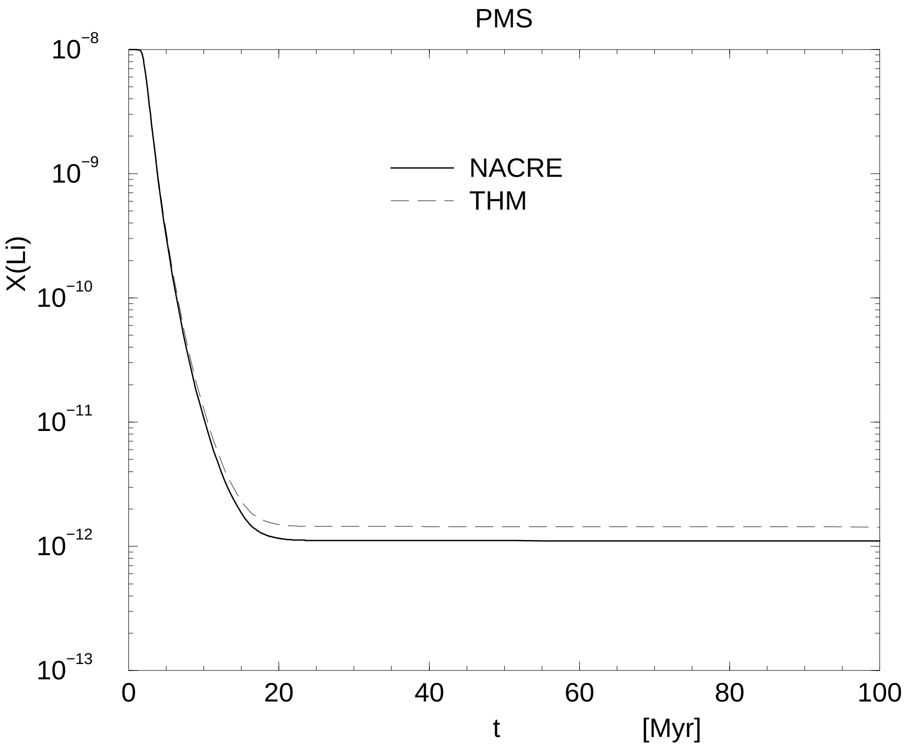

Figure 7.1: Temporal evolution of the lithium surface abundance (expressed in mass fraction) in the Sun, during the PMS phase. The solid line represents a calculation performed using the FRANEC code with the cross section for the $^7Li(p,\alpha)^4He$ taken from [Engstler et al. (1992)]. The dashed line represents the same model calculation with the cross section extracted from the present work.

In figure 7.2 the calculation of the lithium surface abundance in the Sun is shown as a function of time (in units of 10^6 years). As for the PMS case the solid curve represents the calculation with the NACRE [Angulo et al. (1999)] cross section; the dashed line represents the model with the THM cross section. As for the PMS calculation the discrepancy, due to the use of the two different cross sections, is negligible. The dotted vertical line represents the present age of the Sun ($\tau \approx 4.6 \times 10^9$ years).

Thus our models deplete more lithium than expected from observations for both choices of the $^7Li(p,\alpha)^4He$ cross section; a possible explanation of this fact can be found in the poor knowledge of the α parameter, especially during the PMS phase which, as we have seen, is crucial for lithium depletion. In this thesis we have assumed (like in other cited models) the same α for both the MS and PMS phases. It has to be stressed that other models [Morel et al. (1997), Swenson et al. (1994)] can give very different results, according to the approximations and input parameters adopted. For our purpose it is important to underline that the results obtained using NACRE compilation and the THM data are essentially similar.

7.2 Other possible solutions to the "Lithium problem"

As we have reported in the previous sections, the present measurement of the $^7Li(p,\alpha)^4He$ S(0)-factor doesn't change significatively the superficial lithium abundance for the Sun, with respect to the NACRE compilation. This confirms of the previously available data since, the result extracted via the THM gives directly the bare cross section.

So the "Lithium problem" for the Sun as well as for the population I and II (and hence the time evolution of the lithium abundance) is not solved even applying the THM. Moreover, the more precise knowledge of nuclear reaction cross sections does not vary the results of astrophysical models, even in the best known case, the Sun. Other mechanisms and uncertainties should be taken into account in order to solve the "Lithium problem":

- efficiency of convection in the external envelope of stars;
- opacities;
- rotation;
- the equation of state;

- the observed metallicity of the different stellar clusters.

A better evaluation of the role and relative weight of each one of these mechanisms will provide more reliable bases to the astrophysical models. Even if a lot of work has been done concerning the astrophysical models and input physics (as we have seen in this thesis, nuclear astrophysics plays, together with atomic and particle physics, a key-role in this scenario) the solution of the lithium problem is still far away. But the large and synergic efforts of the last years allow us to be quite optimistic for the future.

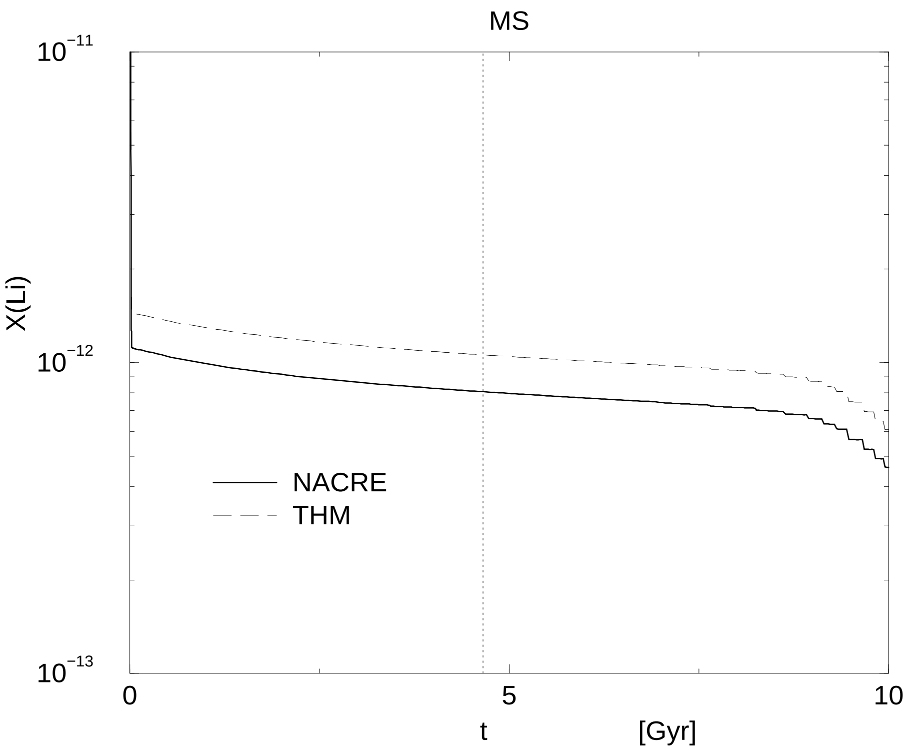

Figure 7.2: Time evolution of the lithium surface abundance (expressed in mass fraction) in the Sun, during the MS phase. The solid line represents a calculation performed using the FRANEC code with the for the $^{7}Li(p,\alpha)^{4}He$ cross section taken from [Engstler et al. (1992)]. The dashed line represent the same model with the cross section extracted from the present work. The dotted vertical line represents the present age of the Sun.

Concluding remarks

The THM: a complementary tool for experimental nuclear astrophysics

By studying the two reactions, $^6Li(d,\alpha)^4He$ and $^7Li(p,\alpha)^4He$, a positive test of validity of the THM is obtained. Thanks to an improved theoretical description of the method, which is reported in this thesis and in [Spitaleri et al. (2000)], the agreement of the indirect and direct [Engstler et al. (1992)] S(E)-factors for both reactions is quite fair over all the explored energy range. Again we stress that the normalization of indirect data do direct ones is required by the method itself; in this sense the THM should be considered as a complementary tool to investigate charged particle reactions at very low energies.

Moreover at very low energies (in the present case at energies E$\leq$100 keV) a discrepancy, between the "direct" and "indirect" data trend, is seen for both reactions; this seems to be essentially due to the electron screening effect, which enhances the S(E)-factor at low energies in direct measurements. Thus the THM becomes a tool for exploring the electron screening effect and to measure, without extrapolations, the bare astrophysical factor.

As a further validity test of the THM analysis a complete coherence is found (see chapter 4) for the $^6Li(d,\alpha)^4He$ for indirect data extracted both from target and projectile break-up [Musumarra et al. (2001)].

Astrophysical implications

The astrophysical factor for both the examined reactions has been extracted. The comparison with direct data shows a nice agreement for both the $^6Li(d,\alpha)^4He$ and $^7Li(p,\alpha)^4He$ data sets. As it was found in chapter 4 the S(0) term of the astrophysical factor for the $^6Li(d,\alpha)^4He$ is 16.9 $\pm$ 0.5 Mev·b while for the $^7Li(p,\alpha)^4He$ S(0)=55 $\pm$ 3keV·b (see chapter 5). This essentially leads to unchanged astrophysical implications with respect to the NACRE compilation [Angulo et al. (1999)].

To evaluate the impact of the new THM data on the lithium problem a study of the solar lithium abundance has been performed, using the FRANEC code. It was calculated for both the PMS and MS phase of solar evolution for two different values of the $^7Li(p,\alpha)^4He$ cross section, the THM and the NACRE one. The difference between the two calculations is around 5%; clearly the THM, being an independent way to measure a bare nucleus cross section, confirms that the uncertainties on the $^7Li(p,\alpha)^4He$ cross section cannot explain the lithium problem, whose possible solution are briefly reviewed at the end of chapter 7.

The electron screening: a systematic discrepancy?
By measuring the bare nucleus astrophysical S(E)-factor using the THM we can measure, without extrapolation, the electron screening potential. This has been done for the two examined reactions in chapters 4 and 5 respectively.

For the $^6Li(d,\alpha)^4He$ reaction, after averaging data extracted from target and projectile break-up, we have measured U_e=320 ± 50 eV. This is in fair agreement with the directly measured value U_e=330 ± 120 eV [Engstler et al. (1992)], while the adiabatic limit is U_{ad}=186 eV.

The electron screening potential energy for the $^7Li(p,\alpha)^4He$ reaction has been also extracted, after averaging over all the data available. A final value of U_e=330 ± 40 eV has been obtained. The comparison with the direct measurement [Engstler et al. (1992)], U_e=300 ± 160 eV, shows also in this case a nice agreement.

As for the $^6Li(d,\alpha)^4He$ case the adiabatic limit produces U_{ad}=186 eV; this confirms a systematic discrepancy between the experimental values and the theoretical predictions. Possible solutions to this discrepancy (which has been observed in other reactions as well, e.g. [Engstler et al. (1992), Costantini et al. (2000)]) have been described in section 2.5.1. The THM results, at least for the two studied reactions, clearly shows that the extrapolations were correct; thus a possible solution can be found either in the description of atomic physics or in the extrapolations used to describe the energy loss in the target at very low energies (E≤50 keV). These problems are currently under investigation.

By comparing the two results obtained in this thesis for both the $^6Li(d,\alpha)^4He$ and $^7Li(p,\alpha)^4He$ reactions, we obtain an agreement that can be explained by referring to the "isotopical independence" of the electron screening effect, i.e. the fact that the screening potential doesn't depend on the mass number but only on the number electrons of the interacting particles. This confirms previous results [Engstler et al. (1992)] and the available microscopic description of the screening effect.

Perspectives

In order to have a complete knowledge of nuclear reactions involved in lithium depletion, the study of the $^6Li(p,\alpha)^3He$ reaction (by using the THM) has already been started. The evaluation of its screening potential could give a more complete overview of this problem. At the same time the energy loss trend at astrophysical energies is currently under investigation in Bochum.

In this framework the THM can play a key role for obtaining information, without any extrapolation, on the bare astrophysical S(E)-factor and the electron screening effect. Its complementarity to direct measurements will certainly give an important contribution to nuclear astrophysics and to the electron screening problem.

Acknowledgements

At the end of this very nice experience, which has been my Ph.D. course I feel to thank all the people who have helped me. My tutor, Prof. C. Spitaleri, above all, for his constant guidance during these years. Then my best acknowledgements are for Maria Grazia whose help has been crucial during the completion of this work. I also thank Pierpaolo, Agatino, Aurora, Alessia, Stefano, Prof. Lattuada and Prof. Zappalà for sharing their knowledge with me and for their kindness in helping me in many occasions.

I wish to thank all the people who have helped me during the periods abroad: their contribute was important not only for useful discussions but for spending really nice periods in foreign Institutions. My thanks are due to Prof. D. Miljanić, M. Milin and N. Soic from Rudjer Boskovic Institut (Zagreb), S. Cherubini (Louvain-la-Neuve), Prof. H. Wolter, S. Typel and T. Gaitanos from LMU (München), Prof. Rolfs and M. Aliotta from Ruhr Universität (Bochum).

I acknowledge here the contribution to this thesis from the Stellar Astrophysics group in Pisa: I wish to thank Prof. Castellani, S. Degl'Innocenti and A. Imperio.

Though the road was difficult during this period I've always believed in its completion thanks to these friends that, without any distinction, I heartfully thank.

Bibliography

[Aliotta et al. (2000)] M. Aliotta, C. Spitaleri, M. Lattuada, A. Musumarra, R. G. Pizzone, A. Tumino, C. Rolfs, F. Strieder, Eur. Phys. J., **9**, 435 (2000)

[Anders & Grevesse (1989)] Anders E. and Grevesse N.: *Geoch. Cosmoch. Acta*, **53**, 197 (1982)

[Angulo et al. (1999)] Angulo, C., et al.: Nucl. Phys. A, 656, 3 (1999)

[Applegate et al. (1988)] Applegate J.H., Hogan C.J. and Scherrer R.J.: Ap. J., **329**, 572 (1988)

[Arnould & Takahashi (1999)] M. Arnould & K. Takahashi:Rep. Prog. Phys.,**62**, 395 (1999)

[Assenbaum et al. (1987)] Assenbaum H.J., Langanke K. and Rolfs C.: Z. Phys., **327**, 461 (1987).

[Baade et al. (1991)] Baade D., Cristiani S., Lanz T., Malaney R.A., Sahu K. and Vladilo G.: Astr. Ap., **251**, 253 (1991).

[Bahcall et al. (1995)] N.L. Bahcall et al.: Ap. J. **447**, L81 (1995)

[Barker (2000)] Barker, F.C.: Phys. Rev. C, 62, 044607 (2000)

[Baur (1986)] Baur G.: Phys. Lett., **B178**, 135 (1986)

[Baur & Rebel (1994)] Baur G. & Rebel H.: J. Phys. **G20**, 1 (1994)

[Bencze (1989)] G. Bencze: Nucl. Phys. **A492**, 459 (1989)

[Bluge (1989)] G.Bluge, K. Langanke, H.G. Reusch, C. Rolfs: Z. Phys., **333**, 219 (1989)

[Bonetti et al. (1999)] R. Bonetti et al.: Phys. Rev. Lett. **82**, 5205 (1999)

[Bracci et al. (1990)] L. Bracci, Fiorentini G., V.S. Melezhik, G. Mezzorani, P. Quarati: Nucl. Phys. **A513**,316 (1990)

[Calvi et al. (1997)] Calvi, G., et al.: Nucl. Phys. **A621**, 139c (1997)

[Castellani et al. (1996)] V. Castellani, G. Fiorentini, B. Ricci, O. Straniero: Z. Phys., **A354**, 237 (1996)

[Castellani et al. (1997)] Castellani V., et al.: Phys. Rep., 281, 309 (1997)

[Cester (1984)] Cester B.: *"Corso di Astrofisica"*, ed. Hoepli (1984)

[Cherubini et al. (1996)] Cherubini, S., et al.: Ap.J., 457, 855 (1996)

[Chew & Wick (1952)] Chew G.F. & Wick G.C.: Phys. Rev. **85**, 636 (1952)

[Ciacio et al. (1997)] Ciacio F., Degl'Innocenti S., Ricci B.: A &A Suppl., 123, 449. (1997)

[Clayton (1983)] D.D. Clayton:*Principles of Stellar Evolution and Nucleosynthesis*, The University of Chicago press, Chicago and London (1983)

[Copi et al. (1995)] C.J. Copi, D.N. Schramm, M.S. Turner: Science **627**, 192 (1995)

[Costantini et al. (2000)] H. Costantini et al.: Phys. Lett. **B482**, 43 (2000)

[D'Antona & Mazzitelli (1994)] D'Antona F.& Mazzitelli I.: Ap. J.S. (1994)

[Delyannis et al. (1990)] C.P. Deliyannis, P. Demarque, S.D. Kawaler: Ap. J. Suppl., **73**, 21 (1990)

[Delyannis et al. (1998)] C.P. Deliyannis et al.: Proc. of Nuclei in the Cosmos, Volos, ed. Frontieres (1998)

[Engstler et al. (1992)] S. Engstler, G. Raimann, C. Angulo, U. Greife, C. Rolfs, U. Schröder, E. Somorjai, B. Kirch and K. Langanke: Z. Phys. **A342**, 471 (1992)

[Evans (1969)] R. D. Evans: *The Atomic Nucleus*, Mc Graw-Hill, (1969)

[Fiorentini et al. (1995)] G. Fiorentini, R.W. Kavanagh, C. Rolfs: Z. Phys. **350**, 289 (1995)

[Gagliardi et al. (1999)] Gagliardi A.C., et al.: Phys. Rev. **C59**, 1149 (1999)

[Jain et al. (1970)] Jain M., Roos P.G., Pugh H.G. and Holmgren H.D.:Nucl. Phys., **A153**, 49 (1970)

[Kippenhahn & Weigert (1990)] R. Kippenhahn & a. Weigert: *Stellar structure and evolution*, Springer-Verlag (1990)

[Langanke et al. (1996)] K. Langanke et al.: Phys. Lett., **B369**, 211 (1996)

[Lattuada et al. (1988)] Lattuada et al.: Z. Phys., **A330**, 183 (1988)

[Lattuada et al. (2001)] M. Lattuada, R.G. Pizzone, S. Typel, P. Figuera, D. Miljanic, A. Musumarra, M.G. Pellegriti, C. Rolfs, C. Spitaleri, H.H. Wolter: in press on Ap.J. (2001)

[Lemoine et al. (1997)] M. Lemoine et al.: Ap. J., **478**, 554 (1997)

[Lindhar (1968)] J. Lindhar: Mat. Phys. Medd. Dan. Vid. Selk., **36**, No 10 (1968)

[Linsky et al. (1993)] Linsky J. L. et al.: Ap. J., **402**, 694 (1993)

[Malaney & Fowler (1988)] Malaney R. A. and Fowler W.: Ap. J., **33**, 14 (1988)

[Malaney & Mathews (1993)] R.A. Malaney and G. Mathews: Phys. Rep. **229**, 147 (1998)

[Mather et al. (1994)] J. Mather et al.: Ap. J. **420**, 439 (1994)

[Michaud & Charbonneau (1991)] G. Michaud and P. Charbonneau: Space Science Review, **57**, 1 (1991)

[Morel et al. (1997)] P. Morel, Provost J., G. Bartholomieu: A &A, 327, 349 (1997)

[Musumarra et al. (2001)] A. Musumarra, R.G. Pizzone, S. Blagus, M. Bogovac, P. Figuera, M. Lattuada, M. Milin, D. Milianič, M.G. Pellegriti, D. Rendic, C. Rolfs, N. Soic, C. Spitaleri, S. Typel, H.H. Wolter and M. Zadro: Phys. Rev. **C64**, 068801,(2001)

[Nollet et al. (1997)] K.M. Nollet, M. Lemoine and D.N. Schramm: Phys. Rev. **C56**, 1114 (1997);

[Olive & Steigman (1995)] Olive K.A. and Steigman G.: Ap. J. Suppl, **97**, 49 (1995)

[Pinsonneault et al. (1990)] Pinsonneault M.H. et al.: Ap. J.S. **74**, 501 (1990)

[Pinsonneault et al. (1992)] M.H. Pinsonneault et al.: Ap. J. Suppl **78**, 179 (1992)

[Rogers & Iglesias (1996)] Rogers F.J., Iglesias C.A., Ap.J., 456, 902. (1996)

[Rolfs & Kavanagh (1986)] Rolfs, C., and Kavanagh R.W.: Nucl. Phys. **A455**, 179 (1986)

[Rolfs & Rodney (1988)] C. Rolfs & W. Rodney:*Cauldrons in the Cosmos*, The University of Chicago press, Chicago (1988)

[Satchler (1990)] Satchler G.R.:*"Introduction to Nuclear Reactions"* II edition, ed. MacMillan (1990)

[Schramm & Turner (1998)] D.N. Schramm and M.S. Turner: Rev. Mod. Phys. **70**, 303 (1998) and references therein

[Shoppa et al. (1993)] T.D. Shoppa, S.E. Koonin, K. Langanke, R. Seki: Phis. Rev. **C48**, 837 (1993)

[Smith et al. (1993)] M. Smith et al.: Ap. J. Suppl. **85**, 219 (1993)

[Soderblom et al. (1993)] Soderblom D.R. et al.: Ap. J. Suppl., **85**, 315 (1986)

[Spitaleri et al. (1999)] Spitaleri, C., Aliotta M., Cherubini S., Lattuada M., Miljanic D., Romano S., Soic N., Zadro M., Zappalà R.A.: Phys. Rev. **C60**, 055802 (1999)

[Spitaleri et al. (2000)] Spitaleri, C., Aliotta M., Figuera P., Lattuada M., R.G. Pizzone, Romano S., Tumino A., Rolfs C., Gialanella L., Strieder F., Cherubini S., Musumarra A., Miljanic D., Typel S., Wolter H.H.: European Physical Journal, **7**, 181 (2000)

[Spitaleri et al. (2001)] C. Spitaleri, S. Typel, R.G. Pizzone, M. Aliotta, S. Blagus, M. Bogovac, S. Cherubini, P. Figuera, M. Lattuada, M. Milin, D. Milianič, A. Musumarra, M.G. Pellegriti, D. Rendic, C. Rolfs, S. Romano, N. Soic, A. Tumino, H.H. Wolter, M. Zadro: Phys. Rev., **C63**, 055801 (2001)

[Spite & Spite (1982)] F. Spite and M. Spite: Astr. Ap., **115**, 357 (1982)

[Spite et al. (1996)] M. Spite et al.: A. & A. **307**, 172 (1996)

[Swenson et al. (1994)] F.J. Swenson, J. Faulkner, F.J. Rogers and C.A. Iglesias: Ap. J. **425** 286 (1994)

[Thorburn et al. (1993)] A.J. Thorburn et al.: Ap. J., **421**, 828 (1993)

[Thorburn et al. (1994)] A.J. Thornburn at al.: Ap. J. **415**, 150 (1994)

[Typel & Wolter (2000)] S. Typel and H. H. Wolter: Few-Body Systems **29**, 75 (2000)

[Vangioni-Flam et al. (2000)] E. Vangioni-Flam et al.: A. & A. **360**, 15 (2000)

[Warner et al. (1987)] R.E. Warner, B.A. Vaughan, J.A. Ditusa, J.W. Rovine, R.S. Wakeland, C.P. Browne, S.E. Darden, S. Sen, A. Nadasen, A. Basak, T.R.

Donoghoue, T. Rinckel, K. Sale, G.C. Ball, W.G. Davies, A.J. Ferguson, J. Forster: Nucl. Phys. **A470**, 339 (1987)

[White et al. (1986)] White R.E.: *Ap. J.*, **307**, 777 (1986)

[Yang et al. (1984)] J. Yang et al.: Ap. J., **281**, 493 (1984)

[Zadro et al. (1989)] Zadro, M., Miljanić, D., Spitaleri, C., Calvi, G., Lattuada, M., Riggi, F.: Phys. Rev. **C40**, 181 (1989)